

The Mass Budget of Planet Forming Discs: Isolating the Epoch of Planetesimal Formation

J. R. Najita^{1,2*} and S. J. Kenyon²

¹*National Optical Astronomy Observatory, 950 Cherry Avenue, Tucson, AZ. 85719, USA*

²*Harvard-Smithsonian Center for Astrophysics, 60 Garden Street, Cambridge, MA 02138, USA*

ABSTRACT

The high rate of planet detection among solar-type stars argues that planet formation is common. It is also generally assumed that planets form in protoplanetary discs like those observed in nearby star forming regions. On what timescale does the transformation from discs to planets occur? Here we show that current inventories of planets and protoplanetary discs are sensitive enough to place basic constraints on the timescale and efficiency of the planet formation process. A comparison of planet detection statistics and the measured solid reservoirs in T Tauri discs suggests that planet formation is likely already underway at the few Myr age of the discs in Taurus-Auriga, with a large fraction of solids having been converted into large objects with low millimeter opacity and/or sequestered at small disc radii where they are difficult to detect at millimeter wavelengths.

Key words: planets and satellites: formation – protoplanetary discs – stars: formation –

1 INTRODUCTION

Throughout the galaxy, nearly every young star is born with an opaque circumstellar disc of gas and dust (Haisch et al. 2001; Mamajek 2009; Williams & Cieza 2011). Among T Tauri stars in the Taurus-Auriga dark cloud with ages of a few Myr (Luhman et al. 2010), the discs have outer radii of 30–200 AU and masses of roughly 3×10^{-4} to 0.25 times the mass of the central star (Andrews et al. 2013). By the time stars reach ages of 10–15 Myr, only a few show some evidence for large amounts of gas or dust (see also Hernández et al. 2007; Currie et al. 2009; Kennedy & Kenyon 2009; Espaillat et al. 2014). In the rest, the gas and dust have disappeared.

In current theories of star and planet formation, various physical processes convert the gas and dust surrounding young stars into planetary systems (e.g., Youdin & Kenyon 2013). In the popular core accretion picture, the dust grains in discs are first transformed into planetesimals, the building blocks of planets (e.g., Goldreich & Ward 1973; Weidenschilling 1980; Youdin & Chiang 2004; Rice et al. 2004, 2006; Johansen et al. 2007; Birnstiel et al. 2010; Youdin 2011a; Windmark et al. 2012; Garaud et al. 2013). Planetesimals then grow collisionally to produce terrestrial planets and the solid cores of giant planets (e.g., Wetherill & Stewart 1993; Pollack et al. 1996). Throughout this agglomeration process, several mechanisms – gas

drag, type I migration, and scattering – can cause large grains, planetesimals, or planets to migrate through the disc (Adachi et al. 1976; Weidenschilling 1977a; Malhotra 1995; Rasio & Ford 1996; Ward 1997; Jurić & Tremaine 2008). Currently, there is little agreement on the relative timing of growth and migration for known exoplanets observed close to their host stars. In one scenario, grains and planetesimals migrate inward and then grow into massive planets more or less *in situ* (e.g., Hansen & Murray 2012; Chiang & Laughlin 2013; Hansen & Murray 2013). Alternatively, massive planets might first grow farther away from the host star and then migrate or scatter inward (e.g., Ida & Lin 2005, 2008a; Kennedy & Kenyon 2008; Mann et al. 2010; Raymond & Cossou 2014).

Apart from the theoretical uncertainties, several observations support the notion that planets form in discs surrounding T Tauri stars. The mass of the ‘minimum mass solar nebula’ (MMSN) – the minimum amount of material required to produce the planets in the solar system – lies within the observed mass range of T Tauri discs with ages of a few Myr (Weidenschilling 1977b; Hayashi 1981; Chiang & Youdin 2010; Andrews et al. 2013). Many stars with ages of 10 Myr and older are surrounded by optically thin rings or discs of dusty debris (Wyatt 2008; Matthews et al. 2014). For ensembles of stars with a broad range of ages, the properties (mass, temperature, and frequency) of dusty debris discs are consistent with the expected evolution of an ensemble of invisible 10–100 km objects left over from the formation of much larger planets

* E-mail: najita@noao.edu (JRN)

(Kenyon & Bromley 2008, 2010; Kennedy & Wyatt 2010). Sensitive direct images of several of these systems reveal Jupiter mass planets (Marois et al. 2008; Lagrange et al. 2010) which may sculpt the disc (e.g., Wyatt et al. 1999; Wilner et al. 2002; Stark & Kuchner 2009; Thebault et al. 2012). Searches for planets using microlensing, radial velocity, and transit data also detect an amazing diversity of planets orbiting older stars (e.g., Howard et al. 2010; Sumi et al. 2011; Howard et al. 2012). The masses of these planetary systems lie within the known mass range of T Tauri discs. Thus, it seems obvious that exoplanets form out of T Tauri discs.

Despite this clear picture, the high incidence rates of planetary systems (Cumming et al. 2008; Gould et al. 2010; Mayor et al. 2011; Cassan et al. 2012; Batalha et al. 2013; Fressin et al. 2013; Morton & Swift 2013) now appear to challenge the ability of the reservoirs of solids in T Tauri discs to account for the solids bound up in planets and in the parent bodies of debris discs. When T Tauri disc masses were first measured in the 1990s, their masses were safely above the MMSN mass (Beckwith & Sargent 1993; Osterloh & Beckwith 1995). Debris discs and massive planetary systems were relatively rare. Today, improved technology enables a more complete census of protoplanetary disc masses, with clear detections at very low solid masses, $\leq 1\text{--}3\text{ M}_{\oplus}$ (e.g., Andrews et al. 2013). We also now know that nearly all stars have one – possibly more – Earth-mass to Jupiter-mass planet (Gould et al. 2006; Mayor et al. 2011; Youdin 2011b; Cassan et al. 2012; Petigura et al. 2013; Morton & Swift 2013). Moreover, in the three decades since the first discoveries of discs of small dust grains surrounding Vega and β Pic (Aumann et al. 1984; Smith & Terrile 1984), observations have revealed substantial infrared (IR) excesses associated with hundreds of normal main sequence stars and subgiants with ages ranging from a few Myr to 10 Gyr (e.g., Backman & Paresce 1993; Habing et al. 2001; Rieke et al. 2005; Rhee et al. 2007; Greaves & Wyatt 2010; Eiroa et al. 2013; Bonsor et al. 2014; Chen et al. 2014).

Taken together, the plethora of Earth-mass planets and very low mass T Tauri discs suggest a clear need to examine whether the solids available in known ensembles of T Tauri discs are adequate to explain the solids observed in planetary systems surrounding 10 Myr to 10 Gyr old stars. Previous discussions of this issue focus on the ability of massive T Tauri discs to explain the frequency of gas giant planets (e.g., Greaves & Rice 2010; Vorobyov 2011; Williams 2012). Given the theoretical inefficiency of planet formation, gas giants are expected to form in discs more than 2–3 times the MMSN mass (e.g., Dodson-Robinson et al. 2009). Because T Tauri discs of this mass are rarer than giant planets (Andrews & Williams 2005; Cumming et al. 2008), the assumed inefficiency of planet formation implies that planet formation begins before the T Tauri phase.

Recent advances in inventories of discs and exoplanets now allow us to infer the epoch of planet formation more directly. As we describe below, a comparison of the distributions of disc and exoplanet masses from $\sim 1\text{ M}_{\oplus}$ to several M_J leads to the stronger implication that planet formation is likely underway in class II discs *independent of assumptions about the efficiency of planet formation*.

After reviewing current knowledge of the frequency and masses of planets and debris discs around nearby stars (§2),

we examine the most sensitive measurements of the mass available in discs surrounding young stars (§3). Comparing the required mass with the available disc mass (§4) demonstrates that the mass reservoirs in T Tauri discs match the frequency and masses of (i) planets within 1 AU of their host star, (ii) gas giants at 1–10 AU, and (iii) debris discs at ≥ 20 AU from the host star. However, the available mass in T Tauri discs is insufficient to explain the frequency of 5–30 M_{\oplus} microlensing planets at 1–10 AU from the host star. While some factors – measurement errors, planets with negligible core masses, and uncertainties in disc mass – complicate our analysis (§5.1), our approach is conservative (§5.2) and these issues are unlikely to change our conclusions (§6).

2 THE INCIDENCE RATES OF PLANETS AND DEBRIS DISCS

To inventory the solid masses associated with mature planetary systems, we consider the frequency of planets and debris discs around old stars (age \gg few Myr). Robust ground-based and space-based surveys paint a rich picture of planets close to (radial velocity and transit data) and far from (microlensing) the host star. Surveys with *IRAS*, *Spitzer*, and *Herschel* identify debris discs surrounding stars over a range of ages. In this discussion, we focus on results for FGK main sequence stars where the available methods yield fairly large ensembles of debris discs and planets.

2.1 Super-Earths and Neptunes:

Planets in the 1–30 M_{\oplus} mass range are very common. In radial velocity studies with the HARPS spectrograph, $\sim 54\%$ of stars with FGK spectral types have a 1–30 M_{\oplus} planet with an orbital period $P \leq 100$ d (Mayor et al. 2011). Roughly 70% of these planets have masses of 1–10 M_{\oplus} . Only a few percent have a giant planet more massive than 30 M_{\oplus} .

Analyses of *Kepler* data suggest similar results (Dong & Zhu 2013; Petigura et al. 2013; Foreman-Mackey et al. 2014). For planets with $P \leq 100$ d, the incidence rates are 20–30% for 1–2 R_{\oplus} planets and 20–40% for 2–4 R_{\oplus} planets. Using the planet mass-radius scaling for planets in our Solar System ($M_p/M_{\oplus} = (R_p/R_{\oplus})^{2.06}$, Chiang & Laughlin 2013), these two radius ranges correspond to the mass ranges 1–4 M_{\oplus} and 4–17 M_{\oplus} .

These high incidence rates appear to continue to longer periods. Several analyses of low mass *Kepler* planet candidates demonstrate that the incidence rate of planets is approximately constant with $\log P$ (Dong & Zhu 2013; Petigura et al. 2013; Foreman-Mackey et al. 2014). Among low mass planets with radii $R_p \approx 1\text{--}4\text{ R}_{\oplus}$, there are roughly half as many planets detected in the period interval $P = 100\text{--}400$ d as there are with $P \leq 100$ d.

If we extrapolate the HARPS results with orbital period in the same way, the planet incidence rates for $P \leq 400$ d from the HARPS survey are $\sim 27\%$ (1.5–3 M_{\oplus}), $\sim 32\%$ (3–10 M_{\oplus}), and $\sim 22\%$ (10–30 M_{\oplus}). The resulting total incidence rate of 81% in the mass range 1.5–30 M_{\oplus} is similar to the *Kepler* incidence rate of $\sim 75\%$ for the mass range 1–17 M_{\oplus} (Dong & Zhu 2013; Foreman-Mackey et al. 2014). Figure 1 shows the differential incidence rate of planets as a

function of mass from Mayor et al. (2011) after their correction for detection bias and assuming a cumulative incidence rate of 54% for planets with $M_p = 1.5\text{--}30\text{ M}_\oplus$ and $P \leq 100\text{ d}$ (solid orange curve). The differential incidence rate generally increases with decreasing $\log M$ from 30 M_\oplus to 3 M_\oplus .

To supplement these results, we consider several samples of transiting planets from the *Kepler Space Telescope*. After downloading the *Kepler* planet candidates from the first six (Q1–Q6; Batalha et al. 2013) and first eight (Q1–Q8; Burke et al. 2014) quarters of operation, we extracted candidates with signal-to-noise ratios of 8, orbital periods $P \leq 125\text{ d}$, and host star effective temperatures $T_{\text{eff}} = 5000\text{--}6500$ (spectral types of F5–K2 in Kenyon & Hartmann 1995, see also Dong & Zhu 2013). From original samples of 2338 (3864) planets in the Q1–Q6 (Q1–Q8) data, this cut reduced the sample to 1582 (2495) planets orbiting 1251 (2067) host stars.

To derive the incidence rates for *Kepler* planets, we follow several simple steps. For each planet, the mass M_p depends on the radius R_p (Lissauer et al. 2011; Chiang & Laughlin 2013):

$$M_p \approx \left(\frac{R_p}{R_\oplus} \right)^{2.06} \text{ M}_\oplus. \quad (1)$$

Although more detailed mass-radius relations are available (e.g., Seager et al. 2007; Enoch et al. 2012; Lopez & Fortney 2013; Weiss et al. 2013; Weiss & Marcy 2014), these often cover a small range in R_p or require knowledge of the host star metallicity. Equation (1) generally provides a reasonable representation of these more detailed results without introducing additional parameters.

Estimating the mass in solids for these planets requires an algorithm to account for the mass in gas. In the core accretion theory for ice and gas giants, small solids agglomerate into a protoplanet which accretes gas after reaching a mass M_0 (e.g., Pollack et al. 1996; Rogers et al. 2011). A simple estimate for M_s , the mass in solids in every planet, is then

$$M_s = \begin{cases} M_p & M_p \leq M_0 \\ M_0 & M_p \geq M_0 \end{cases} \quad (2)$$

where M_0 is the typical mass of the solid core in a gas giant.

In most theories, M_0 depends on the distance a_f of the growing protoplanet from the host star (Rafikov 2006, 2011; Piso & Youdin 2014). With no observational knowledge of a_f , we adopt two approaches. Our nominal calculations use $M_0 = 10\text{ M}_\oplus$. To allow for a plausible range of M_0 , we also derive mass distributions when M_0 is randomly selected from a range of core masses:

$$M_s = \begin{cases} M_p & M_p \leq M_{0,\min} \\ r(M_{0,\min}, M_p) & M_{0,\min} < M_p < M_{0,\max} \\ M_{0,\max} & M_p \geq M_{0,\max} \end{cases} \quad (3)$$

where $M_{0,\min} = 7.5\text{ M}_\oplus$, $M_{0,\max} = 12.5\text{ M}_\oplus$, and $r(a, b)$ is a random number uniformly distributed on the mass interval (a, b) . This second approach follows the spirit of detailed calculations for the core mass without knowing a_f for each star in the *Kepler* sample. Our conclusions are relatively insensitive to the values of $M_{0,\min}$ and $M_{0,\max}$ (§5.1).

This algorithm agrees reasonably well with observed estimates of heavy element abundances for exoplanets (e.g.,

Torres et al. 2008; Miller & Fortney 2011). In small samples with state-of-the-art analyses, exoplanets have masses in heavy elements of $10\text{--}100\text{ M}_\oplus$. Our adopted core masses lie at the lower limit of this range. Exoplanets are enhanced in heavy elements relative to the host star; the enhancement is correlated with the stellar metallicity. Without robust metallicity estimates for each *Kepler* target, we ignore this correlation.

To compare our *Kepler* results with the Mayor et al. (2011) data, we derive the differential incidence rate for the *Kepler* transiting planets from Batalha et al. (2013) with no correction for the likely gas fraction among planets with $M_p > M_0$. Using the same mass bins and an incidence rate of 54% for $1.5\text{--}30\text{ M}_\oplus$ planets, our derived incidence rates for planets with $P \leq 125\text{ d}$ (Figure 1; solid blue curve) closely follow the HARPS results (Figure 1; orange curve). For $M_p \approx 1.5\text{--}4\text{ M}_\oplus$ and $10\text{--}25\text{ M}_\oplus$, the incidence rate of planets from HARPS is larger than the *Kepler* rate. At $4\text{--}10\text{ M}_\oplus$, the *Kepler* incidence rate is somewhat larger than the HARPS rate (see also Dong & Zhu 2013).

The dotted and dashed blue curves in Figure 1 show the incidence rates for solids after correction for the likely gas fraction in massive planets. When $M_0 = 10\text{ M}_\oplus$, all planets with $M_p > 10\text{ M}_\oplus$ have exactly 10 M_\oplus of solids. Thus, the incidence rate for $6\text{--}10\text{ M}_\oplus$ planets jumps by more than 15%; rates for more massive planets fall to zero (dotted blue curve). Adopting a range of core masses, $M_0 = 7.5\text{--}12.5\text{ M}_\oplus$, leaves some planets in the $10\text{--}15\text{ M}_\oplus$ bin (dashed blue curve).

Anticipating the functional form of the mass distributions derived for the discs of T Tauri stars, we derive a cumulative mass distribution $f(> M)$ for the ensemble of *Kepler* planet candidates from Batalha et al. (2013). After estimating M_s for *Kepler* planets with $R_p \geq 1\text{ R}_\oplus$ and $P \leq 125\text{ d}$, the total mass for each system follows from adding the M_s for each planet in the system. This estimate accounts for the multiplicity of each *Kepler* planetary system. After sorting the systems by total mass, we calculate the fraction of systems with total mass $f(> M)$ and normalize the total fraction for all systems to values appropriate for planets with $P \leq 100\text{ d}$ (0.515) and $P \leq 400\text{ d}$ (0.77; Dong & Zhu 2013).

Figure 2 shows the cumulative incidence rate for the total mass of solids in planetary systems from *Kepler*. This result assumes a random distribution of core masses, $7.5\text{--}12.5\text{ M}_\oplus$, and a total incidence rate of 0.77 for planets with $P \leq 400\text{ d}$. Because most of the uncertainty in the cumulative rate lies at the smallest masses, the rate increases from zero for the most massive planets to the total incidence rate for the least massive planets. At the largest masses ($M_s > 10\text{ M}_\oplus$), the curve rises slowly with decreasing mass. After a steep rise at $3\text{--}10\text{ M}_\oplus$ (see also Figure 1), the curve turns over at the smallest masses where the *Kepler* data are less complete (see also Dong & Zhu 2013; Foreman-Mackey et al. 2014).

Changes in the adopted value for the mass of solids in a giant planet have a negligible impact on the incidence rate. Alternative mass-radius relations for exoplanets (e.g., Weiss & Marcy 2014) tend to enhance the incidence rate of $2\text{--}4\text{ M}_\oplus$ planets at the expense of $1\text{--}2\text{ M}_\oplus$ and $4\text{--}10\text{ M}_\oplus$ planets; using these relations steepens the cumulative distribution in the $3\text{--}5\text{ M}_\oplus$ region and flattens the cumulative

distribution at lower masses. Adopting a different range of host star effective temperatures also has a small impact on the derived incidence rates. Because lower mass stars tend to have lower mass planets (Johnson et al. 2010), adding stars with lower effective temperatures raises (lowers) the incidence rate for lower (higher) mass planets.

Analyzing the larger set of exoplanet candidates from Burke et al. (2014) also leads to similar results. With two extra quarters of data, the *Kepler* Q1–Q8 sample contains a larger fraction of smaller (lower mass) planets. Assuming a fixed incidence rate of planets at $1 M_{\oplus}$ (0.515 for $P \leq 100$ d and 0.7725 for $P \leq 400$ d), the Q1–Q8 sample thus yields a somewhat smaller (larger) incidence rate at large (small) masses. Without a detailed analysis of the *Kepler* detections as in Dong & Zhu (2013), however, the cumulative Q1–Q8 incidence rate is uncertain. Lacking a robust normalization for the Q1–Q8 data, we adopt results from the Batalha et al. (2013) sample.

Given the good correspondence of the uncorrected *Kepler* (solid blue curves) and HARPS (orange curves) incidence rates in Figure 1, the *Kepler* rates with corrections for the gas mass fraction (Figure 1, dotted and dashed blue curves) provide a reasonable estimate for the incidence rate for solids in known short-period exoplanets. Our approach explicitly includes the observed multiplicity of planets among *Kepler* host stars. In the rest of the paper, we use the *Kepler* results with a 7.5–12.5 M_{\oplus} range in core masses to represent the population of planets with $P \leq 400$ d (Figure 2).

To add information on the frequency of super-Earths and Neptunes at larger a , we include results from comprehensive microlensing surveys (e.g., Gould et al. 2010; Cassan et al. 2012). Although the incidence rate of planets with $P \approx 100$ –400 d is approximately constant with $\log P$, microlensing planet searches suggest a rapid increase in the incidence rate at much larger orbital periods. For orbital distances $a \approx 0.5$ –10 AU, the derived planet incidence rates from microlensing, $52^{+22}_{-19}\%$ for 10–30 M_{\oplus} planets and $62^{+35}_{-37}\%$ for 5–10 M_{\oplus} planets, are much larger than incidence rates at smaller a (Cassan et al. 2012). Figure 2 compares the incidence rate of the 5–10 M_{\oplus} and the 10–30 M_{\oplus} microlensing populations (two lower mass open magenta boxes) with the *Kepler* $P \leq 400$ d cumulative incidence rate (green curve). The width of each open box represents the mass range associated with each incidence rate. The solid violet squares indicate the solid masses that are plausibly associated with these populations. Because published microlensing analyses select for binary events consisting of a star and a planetary-mass companion, the microlensing incidence rates apply to systems without a stellar companion within 100 AU.

2.2 Giant Planets:

While only 2–3% of stars host a giant planet within 100 d (Cumming et al. 2008; Mayor et al. 2011; Dong & Zhu 2013), the incidence rate of giant planets grows with orbital separation. Radial velocity surveys directly probe the frequency of gas giant planets for orbital periods $P = 2$ –2000 d (Cumming et al. 2008; Mayor et al. 2011). Extrapolating the $d \log M/d \log P$ distribution to longer periods suggests a giant planet incidence rate of 17%–20% within 20 AU (Cumming et al. 2008).

Microlensing studies also derive large incidence rates for giant planets. Among K–M dwarfs in the Galaxy, $17^{+6}_{-9}\%$ have a Jupiter-mass planet (0.3 – $10 M_J$) with $a \approx 0.5$ –10 AU (Cassan et al. 2012). Over a similar range of masses and semimajor axes, Gould et al. (2010) derive a frequency of $36 \pm 15\%$. Although this orbital period range is somewhat larger than the range probed directly by radial velocity surveys, the extrapolated rate from Cumming et al. (2008) agrees remarkably well with the microlensing rates (see also Gould et al. 2010; Clanton & Gaudi 2014).

Figure 2 compares the incidence rates for gas giants from radial velocities (Cumming et al. 2008; open deep blue box) and from microlensing (Cassan et al. 2012; highest mass open magenta box) with the *Kepler* $P \leq 400$ d rates (green curve). The width of each open box represents the mass range associated with each incidence rate. To inventory only the solids associated with these populations, we adopt a solid core mass of $10 M_{\oplus}$ for both the radial velocity and microlensing giant planet populations. The incidence rates are shown as filled squares centered at this value.

As shown in Figure 2, the two independent estimates of the giant planet incidence rate at 1–20 AU (from radial velocities, solid deep blue box; and microlensing, lowest solid violet box) agree to $\pm 2\%$. These rates are only a few percent larger than the frequency of $> 10 M_{\oplus}$ *Kepler* planets with $a \leq 1$ AU (green curve).

For 5–30 M_{\oplus} planets, the differential incidence rate from microlensing (upper two solid violet squares) is clearly much larger than the HARPS or *Kepler* rates for planets at $P \leq 400$ d. Both of these rates are also much larger than the rates for gas giants. Overall, these two microlensing samples represent the largest reservoirs of super-Earth and Neptune mass planets.

2.3 Debris Discs

With typical fractional luminosities of $L_d/L_{\star} \approx 10^{-5}$ to 10^{-3} , the IR excesses of debris disc systems require as much as a few lunar masses in small ($1 \mu\text{m}$ to 1 mm) dust grains (Backman & Paresce 1993; Wyatt 2008; Matthews et al. 2014). Typical temperatures of 50 K to 300 K imply rings or discs of dust at distances of a few AU to a few hundred AU from the host star (Wyatt 2008; Chen et al. 2014). Because radiation pressure and destructive collisions remove small particles on short time scales, these high frequencies require an invisible supply of material (i.e., larger “parent bodies”) to replenish the dust. Planetesimals with radii of 1–100 km are an obvious choice (Aumann et al. 1984). In this picture, a cascade of collisions among 1–100 km and smaller objects produces the 1–1000 μm particles that emit the IR excess. As the cascade proceeds, radiation pressure ejects 1–10 μm particles from the disc. Over time, the cascade removes nearly all of the material originally present in the 1–100 km parent bodies.

The commonality of debris discs suggests that many stars harbor large reservoirs of solids at distances beyond 20–30 AU (Wyatt 2008; Kenyon & Bromley 2008; Krivov et al. 2008; Kenyon & Bromley 2010; Kennedy & Wyatt 2010). Extensive surveys with *IRAS*, *ISO*, and *Spitzer* find debris discs around 10% to 20% of solar-type main sequence stars (Bryden et al. 2006; Trilling et al. 2008; Carpenter et al. 2009; Sierchio et al. 2014). Deeper surveys with *Herschel*

also identify debris discs associated with roughly 20% of solar-type main sequence stars (Eiroa et al. 2013).

Recent data suggest that the frequency of debris discs is fairly independent of local environment. Among all FGK stars, single and binary stars are equally likely to have debris discs (Trilling et al. 2007). For FGK stars with known planets, the incidence rate of $\sim 29\%$ is similar to the rate of $\sim 20\%$ for all FGK stars (Eiroa et al. 2013; Marshall et al. 2014, see also Bryden et al. 2009). Among the planet-bearing population, debris discs are more common in systems with low mass planets (6/11 systems with $M_p \leq 30 M_\oplus$) than with higher mass planets (5/26 systems with $M_p > 30 M_\oplus$).

From analytic and numerical calculations, explaining the frequency and level of debris disc emission requires 10–100 M_\oplus of solids in parent bodies beyond 10–30 AU (Habing et al. 2001; Wyatt 2008; Kenyon & Bromley 2008, 2010; Kennedy & Wyatt 2010; Gáspár et al. 2013). Thus, the current picture of debris disc evolution eliminates the 10–100 M_\oplus stored in parent bodies from the solid reservoir available to make the known exoplanets (Wyatt 2008; Kenyon & Bromley 2008; Krivov et al. 2008; Raymond et al. 2011).

To place the mass distribution of debris discs on the same footing as exoplanets, we adopt a simple prescription. We assume the debris disc incidence rate from *Herschel* of $\sim 20\%$ among solar-type stars. We also assume that a debris disc indicates at least 10 M_\oplus in 1–100 km objects. Explaining observations of debris discs therefore requires that 20% of solar-type stars have at least 10 M_\oplus in solids which does not participate in the formation of Earth-mass and larger planets. For a first comparison, we assume that this 20% is distributed among systems with 10–20 M_\oplus in solids (Fig. 2; orange box). The placement of the orange box suggests that debris discs require a large amount of mass, comparable to the mass required for gas giants and short period exoplanets from HARPS and *Kepler*.

Overall, the fraction of stars with debris discs beyond 20–30 AU is comparable to the fraction of stars with gas giant planets within 20 AU (Fig. 2; orange and blue boxes). The frequency of both groups is also similar to the fraction of 10 M_\oplus or larger planets within roughly 1 AU. Each of these fractions is much smaller than the fraction of 5–30 M_\oplus planets detected with microlensing.

3 RESERVOIRS OF SOLIDS IN PROTOPLANETARY DISCS

For more than fifty years, the Taurus-Auriga molecular cloud has been the gold standard of low mass pre-main sequence stellar evolution (see, for example, Cohen & Kuhi 1979; Kenyon & Hartmann 1995; Kenyon et al. 2008; Luhman et al. 2010, and references therein). With roughly 350 fairly isolated young stars that span a range of evolutionary stages, Taurus-Auriga has become a popular laboratory to investigate the properties of young stars and their circumstellar discs. Although other star-forming regions (e.g., IC 348, ρ Oph, and the Sco-Cen association) also provide vital information on the evolution of pre-main sequence stars and their discs (e.g., Andrews & Williams 2007; Herbst 2008; Preibisch & Mamajek 2008; Wilking et al. 2008; Williams & Cieza 2011), the physical properties of the

discs in these regions are fairly similar to the larger ensemble of discs in Taurus-Auriga (e.g., Andrews et al. 2013).

In our analysis, we rely on previous classifications of the evolutionary state of the central pre-main sequence star in each system. From analyses of spectral energy distributions (SEDs) (e.g., Adams et al. 1987), stars are divided into class I (protostar, a central star surrounded by a disc and an infalling envelope), class II (classical T Tauri star, a central star surrounded by an opaque disc, with little or no envelope), and class III (weak emission T Tauri star, a central star with little or no disc and envelope). Class I protostars constitute roughly 10% of the complete Taurus-Auriga sample and have typical lifetimes of ~ 0.3 Myr (Offner & McKee 2011); class III sources comprise roughly 25% of the complete class II + III population for solar-type stars (Luhman et al. 2010). The discs in class II sources are commonly assumed to be close analogues of the discs from which the solar system and the known exoplanets formed (e.g., Hueso & Guillot 2005; Ida & Lin 2005; Bromley & Kenyon 2011; Raymond et al. 2011).

Submillimeter continuum observations constrain the mass of solids in nearby circumstellar discs. Andrews et al. (2013) report disc masses for an extensive sample of Class II stars in Taurus-Auriga. Based on the Luhman et al. (2010) study, this sample is statistically complete for stellar spectral types earlier than M8.5. Although Andrews et al. (2013) exclude class I and class III sources from their analysis, Andrews & Williams (2005) summarize disc masses for a less complete set of class I, II, and III objects.

The Andrews et al. (2013) disc masses M_d assume a simple relation between disc mass and submillimeter flux:

$$M_d = \frac{d^2 F_\nu}{\kappa_\nu B_\nu(T_c)} \quad (4)$$

where F_ν is the submillimeter flux density, d is the distance, κ_ν is the opacity, and $B_\nu(T_c)$ is the Planck function at a characteristic temperature T_c that depends on the stellar luminosity. The main uncertainties in disc masses result from uncertainties in T_c and the dust opacity (see Andrews et al. 2013), the latter arising in part from uncertainties in the composition and compactness of the solids. Although these uncertainties have little impact on our analysis, we return to them in §5.

The resulting cumulative distribution of Class II disc masses as a fraction of the stellar mass $f(> M_d/M_*)$ rises approximately linearly with decreasing $\log M_d$, from an upper mass limit of $M_d \sim 0.05 M_*$, down to a lower mass limit of $M_d \sim 0.00015 M_*$ where it reaches unity (Fig. 3, grey curves for a stellar mass of 1 M_\odot). Because Andrews et al. (2013) assume a gas-to-dust ratio of 100 (Andrews & Williams 2005), these upper and lower limits correspond to disc solid masses of $M_s = 167 M_\oplus$ and $0.5 M_\oplus$ for a 1 M_\odot star. The median disc in the sample has a mass of $M_d = 0.003 M_\odot$ in gas and $M_s = 10 M_\oplus$ in solids. Some 70% of discs have masses larger than $M_d > 0.0008 M_\odot$ or $M_s > 2.7 M_\oplus$.

The class II disc mass distribution includes both single, binary, and multiple star systems. In contrast, the HARPS and microlensing studies explicitly exclude stellar binaries (Mayor et al. 2011; Cassan et al. 2012). Because discs in binaries are typically less massive than discs in single stars (Jensen & Akeson 2003; Andrews & Williams 2005), includ-

ing multiples in the submillimeter sample skews the disc mass distribution to lower masses. However, the impact of a stellar companion on disc mass is a strong function of the binary separation. In Taurus-Auriga, binaries with separations > 300 AU have $880\ \mu\text{m}$ continuum fluxes very similar to those of single stars (Harris et al. 2012). For closer binaries, the fluxes range from 5 times smaller for separations of 30–300 AU to 25 times fainter for separations < 30 AU. These results indicate that an appropriate sample of ‘single’ stars excludes binaries with separations less than 300 AU.

To construct a sample of class II T Tauri stars free of close binaries, we remove known binaries with separations of ≤ 300 AU (Kenyon et al. 2008; Luhman et al. 2010; Kraus et al. 2011) from the Andrews et al. (2013) sample. This conservative cut reduces the complete Andrews et al. (2013) sample from 210 stars to 152 stars. As in Andrews et al. (2013), we use the Kaplan-Meier estimator to derive the mass distribution for a set of sources with clear detections and upper limits. The resulting distribution of Class II single star disc masses $f_s(> M_d/M_*)$ (Figure 3, cyan curve) is slightly steeper than the Andrews et al. (2013) distribution (grey curves). The median mass of $\sim 13\text{ M}_{\oplus}$ is roughly 50% larger than the median disc mass for the complete Andrews et al. (2013) sample. Despite the difference in median mass, the masses for discs in the top 1% and 10% and the bottom 1% and 10% are indistinguishable.

Although the Taurus-Auriga class II sample is nearly complete for spectral types earlier than M8–M9, binary samples are relatively incomplete for stars with spectral types later than roughly M4 (Kraus et al. 2011). To investigate whether $f_s(> M_d/M_*)$ is sensitive to the lower spectral type limit, we created a sample of 95 stars consisting only of apparently single class II stars with spectral types of M4 and earlier. The resulting mass distribution is indistinguishable from the distribution for all spectral types.

As a final attempt to characterize how the mass distribution depends on the evolutionary state of a pre-main sequence star, we consider the impact of the ‘discless’ class III sources in Taurus-Auriga. Submillimeter surveys of these weak emission T Tauri stars are not as complete as those for the classical T Tauri stars (Andrews & Williams 2005; Andrews et al. 2013). However, we can make a simple estimate of the impact of these objects on the mass distribution. Assuming that the class III population (which represents 25% of the combined class II + III population) is discless, we add an ensemble of class III sources with zero disc mass to the complete set of class II sources from Andrews et al. (2013). The resulting mass distribution is shallower (Figure 3, red curve); the median mass drops to roughly 7 M_{\oplus} .

The combined class II + class III mass distribution, shown as the red curve in Figure 3, represents a rough lower limit to the mass reservoir available for planet formation. To set a rough upper limit to this reservoir, the violet curve plots the mass distribution for the Taurus-Auriga class I sources (Andrews & Williams 2005). This distribution is much steeper than the class II or class II + III distributions. The median mass reservoir is $50\text{--}100\text{ M}_{\oplus}$; 90% of the sources have reservoirs of $20\text{--}1000\text{ M}_{\oplus}$. With a median mass of roughly $10\text{--}15\text{ M}_{\oplus}$, the discs in the complete ensemble of class II sources (Figure 3, blue or grey curves) are 5 times less massive than the class I discs.

4 COMPARISON OF SOLIDS IN PLANETARY SYSTEMS AND CLASS II PROTOPLANETARY DISCS

From a comparison of Figures 2 and 3, it is clearly difficult for the class II disc mass budget to account for the solids bound up in the known exoplanet and debris disc populations. With reservoirs of 10 M_{\oplus} required for each of debris discs (Figure 2, orange box), Neptunes in microlensing surveys (Figure 2, middle purple box), and gas giants (Figure 2, deep blue box), and with their respective incidence rates of $\sim 20\%$, $\sim 50\%$, and $\sim 20\%$, it seems clear that any class II + III sample with a median mass of 7 M_{\oplus} is hard-pressed to supply enough material to form even this subset of known exoplanetary systems. Even at the higher median mass of the single star class II sample ($10\text{--}15\text{ M}_{\oplus}$), these three populations alone are a severe burden on the class II mass budget. To consider these conclusions in more detail, we now develop several quantitative comparisons between the solid masses available in protoplanetary discs and the solid masses required for known planetary systems.

In §4.1, we use a simple tally approach that considers the solid masses available in the outer (> 20 AU), inner (< 4 AU), and middle ($4\text{--}20$ AU) regions of the disc, compared with the demands placed on these solid reservoirs by debris discs, Kepler planets, and the remaining planet populations, respectively. In §4.2, we use a Monte Carlo approach to create ensembles of systems with planets and debris discs at their known incidence rates; we then compare the solid mass distribution of the ensembles with that of protoplanetary discs. Compared to a simple tally, the Monte Carlo analysis considers only the total solid mass of each system and ignores the fractional disc mass at different radii that is available to form the planet and debris disc populations.

4.1 A Simple Tally

Only a fraction of the total disc mass is likely to be available to generate specific populations of planets and debris discs. For example, the (i) *Kepler* planets ($M_p = 1\text{--}30\text{ M}_{\oplus}$, $a \leq 1\text{ AU}$, $P \leq 400\text{ d}$), (ii) microlensing planets ($M_p > 5\text{ M}_{\oplus}$, $a \approx 0.5\text{--}10\text{ AU}$, $P \approx 0.35\text{--}30\text{ yr}$), and (iii) debris discs ($a \geq 20\text{ AU}$, $P \geq 100\text{ yr}$) are expected to have formed from solids in the inner, middle, and outer regions of the disc. Therefore, a simple way to compare the solid distributions in planetary systems and protoplanetary discs is to compare the planet mass distribution in 3 radial bins with the disc mass distribution in similar radial bins.

For this comparison, we first separate the single-star class II disc mass reservoir into an outer disc ($> 20\text{ AU}$) that may generate debris and an inner disc ($\leq 20\text{ AU}$) that produces the known planets. This division is motivated by the typical semimajor axis ranges of (i) the parent bodies of debris discs (typically $a \geq 20\text{ AU}$) and (ii) the *Kepler* and microlensing planets ($a \leq 20\text{ AU}$).

To construct these reservoirs, we assume that class II discs have power-law surface density distributions $\Sigma \propto a^{-p}$, with $p = 1.5$ as in the MMSN, and outer radii, $r_{\text{out}} = 50\text{ AU}$. Compared to a flatter $p = 1$ distribution, which is often invoked as characteristic of a steady accretion disc, a surface density distribution as steep as $p = 1.5$ concentrates more of the solids at small radii, an arrangement that helps to

account for the large solid mass that is bound up in the $P < 400$ d planet population (see also Chiang & Laughlin 2013).

If the observed dust emission from debris discs persists over the main sequence lifetime of the host star, analytic and numerical models require solid reservoirs of at least $10 M_{\oplus}$ beyond 20 AU (Figure 4, solid orange box; see Wyatt 2008; Kenyon & Bromley 2008, 2010; Kennedy & Wyatt 2010, and references therein). If $\Sigma \propto a^{-1.5}$ and $r_{out} = 50$ AU, the outer disc (20–50 AU) contains 37% of the total mass in solids. Thus, debris disc systems are then drawn from discs with total solid masses $M_{tot,s}$ at least $1/0.37$ times larger than $10 M_{\oplus}$, $M_{tot,s} \geq 27 M_{\oplus}$ (Figure 4; open orange box). The fraction of discs in the single-star class II distribution with masses in this range ($\sim 40\%$; cyan curve) can easily explain the debris disc incidence rate ($\sim 20\%$; open blue box).

With the outer 37% of the disc mass set aside for debris discs, we now divide the remaining 63% into separate reservoirs for the *Kepler* planets and the microlensing planets. The similarity in the shape of the solid green and cyan curves in Figure 4 suggests that we can reduce the masses of single, class II discs by a factor of 3.5 to achieve a rough match with the incidence rate for *Kepler* planets. For a disc with $\Sigma \propto a^{-3/2}$ and $r_{out} = 50$ AU, 28% ($1/3.5$) of the mass is contained within $a \leq 4$ AU. Therefore, if *every Kepler* planet is drawn from a disc roughly 3.5 times more massive than the planet (Figure 4, dashed green curve), the mass contained in *all Kepler* planets will not overly tax the solid reservoirs in class II discs (Figure 4, cyan curve). Producing the $P \leq 400$ d *Kepler* planets from solids within 4 AU requires some mechanism to concentrate the solids toward smaller disc radii. We return to this point in §5.

Having reserved the inner 28% of the solids ($a \leq 4$ AU) for the formation of the $P \leq 400$ d planet population and the outer 37% of the solids ($a \geq 20$ AU) for the generation of debris discs, we are left with the 35% of solids in the middle region (4–20 AU) of the disc. This reservoir needs to have enough mass to account for the remaining planet populations – super-Earths (5–10 M_{\oplus}), Neptunes (10–30 M_{\oplus}), and gas giants ($> 100 M_{\oplus}$) – located at 0.5–20 AU. To evaluate the ability of this middle disc region to produce these planets, we assume that super-Earths have 5 M_{\oplus} of solids; Neptunes and gas giants each have 10 M_{\oplus} of solids (Figure 4, filled purple boxes). If these planets arise from the middle region of the disc, they are drawn from discs with masses $1/0.35$ larger, $M_{tot,s} \geq 14 M_{\oplus}$ for super-Earths, and $M_{tot,s} \geq 28 M_{\oplus}$ for Neptunes and gas giants (Figure 4, open purple boxes).

The middle disc reservoir can easily manage to explain the frequency of gas giants at 0.5–20 AU. The solids in gas giants require that roughly 17% of discs have masses of $M_{tot,s} \geq 28 M_{\oplus}$. Roughly 40% to 50% of class II discs meet this criterion (Figure 4, cyan curve).

Despite this success, it is impossible for the middle disc reservoir to explain the high incidence rates of super-Earths and Neptunes at 1–10 AU. The super-Earths from microlensing surveys require that 62% of discs have masses of $M_{tot,s} \geq 14 M_{\oplus}$. Fewer than 50% of discs match this constraint. When combined with the 17% incidence rate for gas giants at 1–10 AU, matching the 52% incidence rate of Neptunes is even more challenging. Roughly 40% of class II discs

have $M_{tot,s} \geq 28 M_{\oplus}$, well below the nearly 70% required to explain the incidence rate of exoplanets with $M_s > 10 M_{\oplus}$ (Neptunes and gas giants) at 0.5–10 AU.

Modifying the sizes of the three disc reservoirs cannot change these conclusions. For example, the incidence rate of 5–30 M_{\oplus} microlensing planets requires that *every disc* have at least 5 M_{\oplus} in the middle disc region. However, only $\sim 80\%$ of class II sources have this much solid mass in the *entire disc*. Increasing the total mass in the middle disc reservoir by a factor of 2–3 would yield solid masses sufficient to explain the microlensing planets. However, removing this mass from the inner and outer reservoirs leaves little or no (or negative) mass to match the incidence rates for *Kepler* planets or debris discs. Thus, the single star class II disc mass distribution is insufficient to produce the known exoplanets. The gap between these two solid reservoirs is probably broadened by additional factors (e.g., the efficiency of planet formation and undiscovered planet populations; see §5).

4.2 Monte Carlo Simulation

To illustrate the challenges in more detail, we can compare the total solid masses bound up in planets and debris discs with those present in class II discs, independent of how the solids are distributed in radius. For this comparison, we create synthetic distributions of solids in planets and debris discs. Constructing ensembles of planets allows us to make a more general comparison with the mass distribution of T Tauri discs and to evaluate the sensitivity of the results to our set of input assumptions.

To build a simple Monte Carlo simulation, the basic input parameters are the fractions f_j describing the incidence rate for each planet population: the fraction of stars with a debris disc (f_{dd}), gas giant planet (f_{gg}), super-Earth (5–10 M_{\oplus}) microlensing planet (f_{se}), Neptune (10–30 M_{\oplus}) microlensing planet (f_{nep}), or a *Kepler* planet ($f_k(M_s)$). At the start of each simulation, all fractions are fixed, with four of the fractions – f_{dd} , f_{gg} , f_{se} , and f_{nep} – having single values. *Kepler* planets are selected from a table derived from the *Kepler* data described in §2 with a normalization factor $f_{k,0}$ which represents the total fraction of all *Kepler* stars with transiting planets having $P \leq 400$ d (Petigura et al. 2013; Dong & Zhu 2013).

Each planet or debris disc has an assigned mass in solids M_j . For debris discs, gas giants, and microlensing planets, the constant core mass model has $M_{dd} = 10 M_{\oplus}$, $M_{gg} = 10 M_{\oplus}$, $M_{se} = 5 M_{\oplus}$, and $M_{nep} = 10 M_{\oplus}$. *Kepler* planets have masses assigned from eq. (2). To investigate the sensitivity of our results to these parameters, we consider a variable core mass model where we assign a mass range for the core mass and select masses randomly distributed on the mass range as in eq. (3). In this set of models, $M_{dd} = 10$ – $100 M_{\oplus}$, $M_{gg} = 7.5$ – $12.5 M_{\oplus}$, $M_{se} = 2.5$ – $7.5 M_{\oplus}$, and $M_{nep} = 7.5$ – $12.5 M_{\oplus}$. The cores of *Kepler* planets have masses assigned from eq. (3).

To set the fractions, we adopt the observed values described in §2. For debris discs and gas giants, the fractions are straightforward, $f_{dd} = 0.2$ and $f_{gg} = 0.2$. For the *Kepler* planets, we adopt $f_{k,0} = 0.75$ for transiting planets with orbital periods $P \leq 400$ d (Dong & Zhu 2013). Although the nominal fractions for the microlensing planets are $f_{se} = 0.62$ and $f_{nep} = 0.52$, the semimajor axis range

of the microlensing planets, 0.5–10 AU, overlaps with that of the *Kepler* planets ($a \leq 1.05$ AU for $P \leq 400$ d around solar-type stars). Because the *Kepler* incidence rate has a smaller uncertainty, we prefer to use the longer period set of *Kepler* planets than the microlensing planets. To eliminate double-counting, we then need to reduce the microlensing fractions. As guidance, Cumming et al. (2008) show that the frequency of giant planets slowly increases with orbital period beyond $P = 300$ d. Although the *Kepler* data suggest an incidence rate that is roughly constant with $\log P$ for $P = 100$ –400 d (e.g., Petigura et al. 2013; Dong & Zhu 2013), the variation of the incidence rate with P beyond 400 d is unknown. For simplicity, we assume the incidence rate is independent of period, implying $f_{se} = 0.59$ and $f_{nep} = 0.49$ for $a = 1$ –10 AU.

To run the simulation, we draw random numbers r_j ($j = 1$ –5) and select the constant core mass model for the *Kepler* mass distribution. Four random numbers establish the presence or absence of a debris disc, a gas giant, or a microlensing planet:

$$p_j = \begin{cases} 1 & r_j \leq f_j \\ 0 & r_j > f_j \end{cases} \quad (5)$$

where $j = 1$ (debris disc), $j = 2$ (gas giant), $j = 3$ (5 M_\oplus microlensing planet), and $j = 4$ (10 M_\oplus microlensing planet). When $j = 5$ (*Kepler* planet) and $r_j \leq f_{k,0}$, the random number sets the mass of the planet along the *Kepler* mass distribution.

In the constant core mass algorithm, the total mass in planets for the i th star is then

$$M_{t,i} = M_k(p_5) + \sum_{j=1}^4 p_j M_j, \quad (6)$$

where the M_j 's are constant masses for debris discs, gas giants, and microlensing planets.

In the variable core mass algorithm, we draw four additional random numbers and select the variable core mass model for the total mass distribution of *Kepler* planets. The masses M_j ($j = 1$ –4) are then randomly selected on the appropriate range for debris discs, gas giants, and microlensing planets.

After drawing sets of random numbers for N stars, we sort the masses and derive a cumulative mass distribution. Running M trials of N stars allows us to construct a median mass distribution and to estimate the inter-quartile range about this median. Tests with $N = 10000$ and $M = 10000$ demonstrate that the median and inter-quartile range are indistinguishable from the average and dispersion. The inter-quartile range and dispersion are always less than 1%. Thus, the scatter about the median mass distribution is negligible.

The multiplicity statistics of the simulated populations agree well with observations. Roughly 75% of the simulated systems have multiple planets. Approximately 20% of systems with a *Kepler* planet have multiple *Kepler* planets (cf. Rowe et al. 2014; Fabrycky et al. 2014). Among debris disc systems, $\sim 25\%$ have a gas giant, and $\sim 75\%$ have a *Kepler* planet (cf. Marshall et al. 2014).

The Monte Carlo simulations confirm our conclusion that the masses of class II discs are insufficient to explain the masses of all known exoplanets (Figure 5). At large masses (20–30 M_\oplus), the frequency of class II discs (black curve)

is sufficient to explain the incidence rates for debris discs and gas giants in the constant core mass (cyan curve) and the variable core mass (green curve) models. Within this group, somewhat larger core masses for gas giants (up to 20 M_\oplus) and larger maximum masses within the parent bodies of debris discs (up to 200 M_\oplus) still fit within the available mass reservoirs in the most massive class II discs. At smaller masses, however, class II discs cannot explain the high frequency of planets with masses ≤ 5 –10 M_\oplus .

The high frequency of microlensing planets is responsible for the large discrepancy between the mass reservoir required for the known exoplanets and the mass available in class II discs. In a variable core mass model with no 5–30 M_\oplus microlensing planets ($f_{se} = f_{nep} = 0$), class II discs have enough mass to explain the frequency of other known exoplanets (Figure 5, magenta curve). Despite the failure of class II discs to provide enough mass for the known exoplanets, the class I discs have more than enough mass (Figure 5, violet curve), with roughly 3 times the mass required for the known exoplanets.

5 DISCUSSION

Our analysis demonstrates that the solids contained in the single star class II discs of Taurus-Auriga are sufficient to explain the incidence rates for some, but not all, exoplanet populations. The Taurus-Auriga discs have enough mass for *Kepler* planets ($P \leq 400$ d), giant planets ($a \leq 20$ AU), and debris discs (> 20 AU). However, published single star class II disc masses are insufficient to account for the large observed incidence rates of 5–30 M_\oplus microlensing planets (0.5–10 AU). Thus, the mass of solids locked up in planets and the parent bodies of debris discs exceeds the reservoir of solids in the protoplanetary discs commonly assumed to be the starting points of the planet formation process.

In the next sections, we discuss ways to resolve the discrepancy between the observed masses in exoplanets and single star class II discs. After considering possible caveats in our analysis (5.1), we address factors that probably widen the gap between the two mass reservoirs (5.2). We then describe our preferred solution for reconciling the mass budget of protoplanetary discs (§5.3).

5.1 Caveats

There are three main uncertainties in our analysis. Firstly, the microlensing incidence rates have much larger uncertainties than the modest errors in the rates for debris discs and the HARPS and *Kepler* planets. The microlensing results indicate a clear preference for an incidence rate larger than 0 for 5–30 M_\oplus planets (Gould et al. 2006; Cassan et al. 2012). The good agreement between the giant planet (> 100 M_\oplus) incidence rates from microlensing and radial velocity measurements is also encouraging. However, the 3σ error bars for 5–10 M_\oplus and 10–30 M_\oplus planets formally allow any incidence rate between 0 and 1.

In the Monte Carlo simulations of §4.2, we demonstrate that a negligible incidence rate for 5–30 M_\oplus microlensing planets enables a good match between the available mass in single-star class II discs and the mass observed in debris discs at ≥ 20 AU, gas giants at ≤ 20 AU, and *Kepler* planets

at ≤ 1 AU. Simulations with incidence rates of 10% for 5–10 M_{\oplus} and for 10–30 M_{\oplus} planets ($f_{se} + f_{nep} \leq 0.2$) at 1–20 AU also yield reasonable matches with the class II disc mass distribution. For larger incidence rates ($f_{se} + f_{nep} \geq 0.2$), the match is poor. Revised incidence rates with a factor of two reduction in the 1σ error bars would enable a much more accurate assessment of the demand placed on the disc solid mass budget by 5–30 M_{\oplus} planets.

Secondly, we have implicitly assumed the core accretion picture of planet formation, where ice and gas giants have significant solid cores (Pollack et al. 1996). In the disc instability picture (e.g., Boss 2000, 2005), gas giants form in a gravitationally unstable disc and then migrate close to the host star. The viability of this mechanism is uncertain (e.g., Rafikov 2005; Clarke 2009; Rice & Armitage 2009; Kratter et al. 2010; Helled et al. 2013). However, if disc instabilities commonly produce ice and gas giants, our analysis overestimates the solids contained in exoplanets.

To pursue this idea in the Monte Carlo simulations, we define f_{ca} as the fraction of ice and gas giants formed with massive solid cores as in the core accretion model. Disk instabilities must then produce a fraction $1 - f_{ca}$ of ice and gas giants. Although ice and gas giants formed by disc instability may have modest solid cores (Helled et al. 2013), we assume for simplicity that they make no contribution to the mass distributions of solids in exoplanets. The fraction of $>10 M_{\oplus}$ microlensing planets with massive solid cores is $f_{ca}f_{nep}$ for Neptunes and $f_{ca}f_{gg}$ for gas giants. Repeating the Monte Carlo simulations (§4.2) with a variable f_{ca} allows us to measure the importance of the formation pathway in setting the exoplanet mass distribution.

Even with a negligible fraction of ice and gas giants from core accretion, it is impossible to eliminate the discrepancy between the Monte Carlo mass distribution of exoplanets and the single star class II disc mass distribution. For any f_{ca} , the large incidence rate for 5–10 M_{\oplus} microlensing planets precludes a match at small masses, below 5 M_{\oplus} . With $f_{ca} \leq 0.1$, the Monte Carlo results match the observed disc masses above 5 M_{\oplus} . Much larger fractions of giant planets from core accretion (e.g., $f_{ca} \geq 0.2$) yield poor matches in the interval 5–10 M_{\oplus} .

Although we focus on several specific approaches to reduce the mass distribution of exoplanets to the level of the Taurus-Auriga class II sources, some combination of (i) a smaller incidence rate for microlensing planets, (ii) a smaller core mass for planets formed by core accretion, and (iii) a smaller fraction of planets produced by core accretion yields similar results. Among these options, reducing the incidence rate for 5–10 M_{\oplus} microlensing planets is essential. Lowering the incidence rate for 10–30 M_{\oplus} microlensing planets can be combined with the details of the formation mechanism to yield a better match at 5–10 M_{\oplus} .

Finally, the disc masses we use may be underestimated. In contrast to the simple scaling between submillimeter flux and disc mass employed here (eq. [4]; Andrews et al. 2013 and S. Andrews 2014, private communication), a relatively small subset of discs (the brighter submillimeter population) also have mass estimates based on more sophisticated fits to broad-band SEDs and continuum visibilities (e.g., Andrews et al. 2009, 2010, 2011). In approximately half of the systems, the more sophisticated disc masses are larger than the optically thin estimates by factors of 3–8. If these

results were to apply broadly to all Taurus-Auriga discs, our disc masses for single class II sources must be increased by a factor of $\sim 2 - 3$.

However, more sophisticated analyses of the complete ensemble of Taurus-Auriga discs may lead to little change in the median disc mass. Among sources studied to date, disc size generally increases with submillimeter luminosity (Andrews et al. 2010). Larger, brighter discs are therefore cooler than average, requiring more dust to produce the same submillimeter flux. They are therefore expected to have the *largest* corrections to the disc masses derived from the simple optically thin relation (eq. [4]). If the trend of disc size with submillimeter luminosity also applies at very low submillimeter fluxes, the fainter discs are smaller than average and they will tend to have smaller masses than eq. (4) predicts. The true disc mass distribution may then be broader than the distribution derived from eq. (4), extending to both higher and lower disc masses, without altering the median disc mass. Fits to SEDs and visibilities from interferometric observations of the faint disc population are needed to address this issue.

5.2 Exacerbating Factors

While the factors described above can reduce the high frequency of disc solid masses in the 1–20 M_{\oplus} range, other issues probably increase it.

The ensemble of known planets with $M_p \leq 5 M_{\oplus}$ is incomplete. For radial velocity and transit observations, selection effects and sensitivity limit the population of planets with $M_p \leq 1-2 M_{\oplus}$ at $a \leq 1$ AU (e.g., Mayor et al. 2011; Youdin 2011b; Dong & Zhu 2013; Burke et al. 2014). The sensitivity of published microlensing observations precludes planet detections for $M_p \leq 5 M_{\oplus}$ at 1–10 AU (e.g., Gould et al. 2006, 2010; Sumi et al. 2011; Cassan et al. 2012). Because the number of planets grows rapidly with decreasing mass down to 5 M_{\oplus} (Figure 1), we expect that enhancing the sensitivity for microlensing, radial velocity, and transit observations would enable many detections of lower mass planets. Increasing the population of low mass planets in our analysis would add to the discrepancy between the mass in exoplanets and the disc masses in single class II sources.

The population of exoplanets beyond 20 AU is also incomplete. This region is inaccessible to microlensing, radial velocity, and transit techniques. Robust detections from direct imaging are limited to massive planets orbiting young host stars (e.g., Marois et al. 2008; Lagrange et al. 2010; Kraus & Ireland 2012; Currie et al. 2014). Analyses of existing detections and null results from extensive imaging surveys of solar-type stars suggest maximum incidence rates for gas giants of $\sim 10\%$ at $a \geq 20$ AU (Nielsen & Close 2010; Janson et al. 2012; Biller et al. 2013; Yamamoto et al. 2013). If gas giants are roughly half as common as debris discs beyond 20 AU, it is much harder for single class II sources to have enough mass for planets at smaller semimajor axes. Direct imaging technology on the largest ground-based telescopes is improving rapidly (e.g., Hugot et al. 2012; Jovanovic et al. 2013; Macintosh et al. 2014). New exoplanet imagers (GPI, SCExAO, and SPHERE) should enable better estimates for incidence rates of gas giants around young stars. As these estimates improve, it will be easier to

assess the impact of exoplanets beyond 20 AU on the mass budget of the exoplanet population.

As discussed in §3, the single star class II disc mass distribution excludes the class III sources. Comprising roughly 25% of the T Tauri stars in Taurus-Auriga, the class III sources have little or no evidence for large reservoirs of solids (Andrews & Williams 2005). Including these discless stars in the class II disc mass distribution greatly reduces the frequency of T Tauri discs with enough solids to produce the known exoplanets (Figure 3, red curve).

This argument assumes that class III objects are similar in age to class II objects, despite the difference in their evolutionary state. An overlapping age distribution for class II and III objects seems reasonable for Taurus-Auriga, where the class IIs are intermixed with the class IIIs in the HR diagram (Cohen & Kuhl 1979; Kenyon & Hartmann 1995; Güdel et al. 2007). The spatial distributions of class II and class III sources are also similar (Luhman et al. 2010). Although commonly accepted today, future observations may alter this picture. An HR diagram for all of the sources in the new, more complete Luhman et al. (2010) sample may show that a significant fraction of the class III objects are older than the average class II object. Similarly, parallax distances measured with Gaia may reveal that class III objects are closer than the class II objects and therefore older, on average (e.g., Bertout et al. 2007). In assuming that class II and III objects have similar ages, our discussion here represents a worst case scenario.

However, the disposition of the class III sources depends on our uncertain knowledge of their initial state. If class III sources formed with little or no mass in a disc, then their weak submillimeter emission is intrinsic. It is then appropriate to add their negligible solid masses to the class II mass distribution, widening the discrepancy between the ‘initial’ mass distribution of single class II+III sources and the ‘final’ mass distribution of exoplanets.

Alternatively, class III sources could have formed with substantial disc masses and evolved rapidly into their current discless state. If this evolution converted small grains into planetesimals or planets, then it is appropriate to augment the class II mass distribution with the ‘original’ disc masses of the class III sources. If these original disc masses exceed the median disc mass, then class III sources reduce the discrepancy between the initial and final mass distributions.

Searches for reservoirs of solids in the class III sources would illuminate their impact on the initial mass reservoirs of T Tauri discs. Although identifying planetesimals in class III sources seems unlikely, measuring the fraction with debris discs or planets would place clear limits on the reservoir of solids orbiting these young stars. As discussed in Cieza et al. (2013), current limits on the IR excesses of WTTS and class III objects place only limited constraints on the mass in solids that may reside in these systems.

Another issue is the efficiency with which disc solids are converted into planetary systems. The solid mass reservoirs in the known exoplanets clearly represent a *lower limit* on the solids initially available in protoplanetary discs. Observations of warm dust at radial distances of 0.5–2 AU from many solar-type stars suggest a clear inefficiency in terrestrial planet formation (e.g., Currie et al. 2007; Rhee et al. 2008; Melis et al. 2010; Chen et al. 2014; Sierchio et al.

2014). Numerical simulations suggest plausible inefficiencies of 10% to more than 25% (e.g., Wetherill & Stewart 1993; Agnor & Asphaug 2004; Kenyon & Bromley 2004; Asphaug et al. 2006; Raymond et al. 2011). If such inefficiencies are typical of the formation of ice and gas giants, initial disc masses must be correspondingly larger.

The large eccentricities (e) of gas giants, Neptunes, and super-Earths from the *Kepler* and radial velocity data imply even larger inefficiencies. Approximately half of the giant planet population ($M > 0.2M_J$) have orbits with $e > 0.2$ (Howard 2013). Super-Earths and Neptunes ($M < 30 - 40 M_\oplus$) have eccentricities up to ~ 0.45 (Mayor et al. 2011). To produce such large e , current theoretical studies favor scattering among massive protoplanets or planets, where interactions between two or more massive planets eject¹ one planet from the system and place another on an eccentric orbit close to the host star (Rasio & Ford 1996; Jurić & Tremaine 2008; Raymond et al. 2010). If this picture is correct, the initial masses of these planetary systems must have been 1.5–2 times more massive than observed today. If some planets are lost because they migrate into their host stars (e.g., Trilling et al. 1998), the initial masses must be even larger.

Dynamical models of the formation of the Solar System suggest a similarly large inefficiency. Assuming core masses of 5–10 M_\oplus for each gas giant and 2–5 M_\oplus for the terrestrial planets, the total mass in solids contained in the planets is roughly 25–45 M_\oplus . Recent numerical simulations require an additional 30 M_\oplus of solids to stabilize the orbits of the gas giants in their current architecture (e.g., Morbidelli 2013, and references therein). This Nice model therefore requires a minimum initial solid disc mass of roughly 55–75 M_\oplus (see also Desch 2007; Dawson & Murray-Clay 2012) – about twice the mass of the planets – to produce what we think of as a ‘typical’ planetary system without a substantial debris disc.

Figure 6 illustrates the impact of inefficient planet formation. More than 40% of the class II discs (30% of class II+III discs) have masses larger than the most minimal MMSN (25 M_\oplus). This minimal MMSN is therefore fairly typical. However, allowing for the maximum core masses of the gas giants and the inefficiency of the Nice model, fewer than 15% of the class II discs have sufficient mass (75 M_\oplus) to produce the planets in the Solar System. The Solar System is then very atypical.

A similar picture arises in models for the formation of the known exoplanets (e.g., Ida & Lin 2008a,b). In their studies of exoplanets within 1 AU of their host stars, Hansen & Murray (2012, 2013) and Chiang & Laughlin (2013) explore the disc surface density distributions required to build the known exoplanet populations *in situ*. Raymond & Cossou (2014) consider whether the exoplanet populations form at larger distances and then migrate inward to their current locations. In either approach, the masses required for these ‘minimum mass exosolar nebulae’ are within the range outlined for the MMSN in Figure 6. The large masses invoked in these scenarios draw from the upper

¹ In some calculations, the ‘ejected’ star is placed on an eccentric orbit with large a . Because this planet is not included in any of our planet reservoirs, it is lost to our census.

10-15% (Hansen & Murray 2012, 2013; Raymond & Cossou 2014) or upper 35% (Chiang & Laughlin 2013) of class II disc masses.

5.3 When Does Planet Formation Begin?

One way to resolve the discrepancy between the solid masses in planetary systems and single star class II discs is to consider the possibility that the submillimeter disc masses are not “primordial” (e.g., Greaves & Rice 2010; Vorobyov 2011; Williams 2012). If the dust distribution evolves significantly on time scales of a few Myr, current measurements underestimate the true solid reservoirs available for planet formation. Because the inner disc is optically thick, concentrating mm-cm-sized solids in the inner disc hides them from submillimeter telescopes. Alternatively, growing solids to km or larger sizes throughout the disc prevents detection. Either explanation implies that more than 50% of the solids in class II discs is already locked up in large particles or is sequestered at small disc radii (or both).

Current data allow either possibility. If small solids are sequestered inside a few AU, then the disc has a steep surface density distribution, $\Sigma \propto a^{-p}$, with large p . Gas drag and other physical processes naturally concentrate grains in the disc (Nakagawa et al. 1986; Youdin & Chiang 2004; Brauer et al. 2008; Birnstiel et al. 2010, 2012; Laibe et al. 2012; Pinte & Laibe 2014), leading to configurations with $p \geq 1.5$ (Birnstiel & Andrews 2014; Laibe 2014). Observationally, the value of p is not well constrained. Although initial interferometric observations were interpreted as evidence for $p \approx 1$ for some T Tauri discs (Andrews et al. 2010), subsequent multiwavelength studies (Pérez et al. 2012) demonstrate real variations in the grain size distribution with radius that make it difficult to constrain p with existing observations (S. Andrews, private communication).

The growth of solids throughout class II discs is also plausible. Inside 30 AU, the time scale for the growth and radial drift of cm-sized particles is short (Rafikov 2003; Youdin & Chiang 2004; Rice et al. 2004, 2006; Clarke & Lodato 2009; Birnstiel et al. 2010, 2012; Windmark et al. 2012; Garaud et al. 2013; Laibe 2014). Some $\sim 90\%$ of the small solid particles in the inner 30 AU can be converted into cm-sized or larger pebbles on timescales of $1 - 3 \times 10^4$ yr (Birnstiel et al. 2010, 2012). Although agglomeration into larger and larger objects may be possible (see Rice et al. 2006; Clarke & Lodato 2009; Windmark et al. 2012; Garaud et al. 2013, and references therein), recent studies focus on models where small solid particles drift radially inward and concentrate in local pressure maxima (e.g., Dittich et al. 2013, and references therein). When the local gas-to-dust ratio reaches values above unity, streaming instabilities concentrate pebbles into aggregates which collapse gravitationally into much larger planetesimals (e.g., Youdin & Goodman 2005; Johansen et al. 2007, 2009; Youdin 2011a). These planetesimals rapidly accrete the pebbles, evolving into $1 - 10 M_{\oplus}$ protoplanets on time scales $\leq 1 - 3$ Myr, comparable to the ages of Taurus-Auriga T Tauri stars (e.g., Rafikov 2005; Ormel & Klahr 2010; Bromley & Kenyon 2011; Lambrechts & Johansen 2012; Chambers 2014).

There is independent evidence for rapid planetesimal formation in the Solar System, based on radiometric anal-

yses of meteorites (e.g., Bizzarro et al. 2005; Kleine et al. 2009; Schulz et al. 2009; Dauphas & Chaussidon 2011; Dauphas & Pourmand 2011; Sugiura & Fujiya 2014). The elemental abundances of the oldest solar system objects – the mm- to cm-sized calcium aluminum inclusions (CAIs) – indicate that these objects formed on time scales ≤ 0.1 Myr during a period when the Sun emitted copious high energy particles and x-rays. Studies place the epoch of CAI formation during the late class I or early class II phase (Dauphas & Chaussidon 2011), with CAIs accumulating into differentiated planetesimals in the next $\sim 1 - 10$ Myr (Kleine et al. 2009; Dauphas & Chaussidon 2011). Thus, the meteoritic record implies that planetesimal formation was well underway at the onset of the class II phase of solar system history.

Our conclusions expand on previous results derived from comparisons of the disc and exoplanet mass distributions (Greaves & Rice 2010, 2011; Vorobyov 2011; Williams 2012). In earlier studies, both of the adopted mass distributions were incomplete at low masses; thus, the studies focused on the ability of the most massive discs to produce the gas giant planets (e.g., Cumming et al. 2008). Because gas giant planet formation is predicted theoretically to be inefficient in concentrating disc material into planets (e.g., Dodson-Robinson et al. 2008, 2009), giant planets are expected to form only in discs with masses $\geq 2 - 3$ times the mass of the MMSN. With few such discs among class II sources, Greaves & Rice (2010) inferred that planet formation begins at an earlier epoch when discs are more massive (see also Vorobyov 2011; Greaves & Rice 2011; Williams 2012).

This inference relies on the assumed (in)efficiency of planet formation, a quantity that is not well known (e.g., Armitage 2003; Ida & Lin 2008a,b; Dodson-Robinson et al. 2009; Fogg & Nelson 2009; Coleman & Nelson 2014). However, as we have shown, the improved statistics for disc and exoplanet masses now allow us to bypass this difficulty. The new data directly imply a mismatch between the masses in $1 - 10 M_{\oplus}$ planets and the masses available in class II discs (§4). Thus, these data lead to the stronger implication that planet formation is underway in class II discs *independent of assumptions about the efficiency of planet formation*.

This discussion suggests that primordial disc masses are probably much larger than the disc masses of single class II sources measured by Andrews et al. (2013). With masses $2 - 5$ times larger, the discs in class I sources contain more than enough mass to explain the masses of exoplanets (Figure 6) and to accommodate a factor of > 2 inefficiency in converting disc solids into planets (§5.2; see also Greaves & Rice 2011). The cumulative disc mass distribution of the “evolutionarily younger” Class I sources is steeper than that of the Class II sources and roughly parallels the Monte Carlo mass distribution derived from the incidence rates for exoplanets (Figure 5). In this picture, Taurus-Auriga protoplanetary discs can be the precursors of exoplanet systems if Class I objects evolve into Class II objects while preserving a large fraction of their disc solids.

Achieving this outcome may be challenging. Throughout the class I and class II phases, stars continue to accrete mass from their discs and to eject disc mass in winds and jets (e.g., Najita & Shu 1994; Hartmann & Kenyon 1996; Hartmann et al. 1998; Offner & McKee 2011; Frank et al.

2014; Turner et al. 2014). If accretion and mass loss remove a significant fraction of the solids from a class I disc, then the disc will not contain enough material to produce the known exoplanets. However, the time scales for agglomeration and radial transport of solids through the disc are much shorter than the time scales for accretion and mass loss. Thus, it seems plausible that known physical processes can concentrate the solids into large planetesimals while gas accretes onto the central star and is ejected in jets and winds.

Once planetesimals form, they may follow several evolutionary paths. Two scenarios plausibly explain the *Kepler* planets: (i) inward migration followed by *in situ* growth into protoplanets inside 1 AU (Hansen & Murray 2012; Chiang & Laughlin 2013) or (ii) growth into protoplanets at several AU followed by inward migration (Ida & Lin 2008a; Chambers 2008; Raymond et al. 2011). Growth at several AU with little or no migration is necessary to explain the microlensing planets (Ida & Lin 2005, 2008a; Raymond et al. 2011; Raymond & Cossou 2014). Finally, negligible radial transport followed by protoplanet growth beyond 10 AU is responsible for most debris discs. Our results suggest that the first step in any of these scenarios – the formation of planetesimals – is already underway in the Taurus-Auriga class II discs.

6 SUMMARY AND CONCLUSIONS

The emerging paradigm of planet formation as a common outcome of T Tauri disc evolution sheds new light on when planet formation begins and/or the efficiency with which it occurs. We have compared the solids present in known exoplanetary systems (exoplanets and debris discs) with the solid reservoirs reported for T Tauri discs, the presumed birthplaces of planets (§2 and §3). For the comparison, we used a simple tally approach that considers the solid masses available in the outer (> 20 AU), inner (< 4 AU), and middle (4–20 AU) regions of the disc, compared with the demands on these solid reservoirs placed by debris discs, *Kepler* planets, and the remaining planet populations, respectively (§4.1). We also used a Monte Carlo approach to create ensembles of systems with planets and debris discs, based on their known incidence rates, and compared the solid mass distribution of the ensembles with that of protoplanetary discs (§4.2). The latter approach only considers the total mass budget of each system and ignores the fraction of the disc mass at different disc radii that might be available to form the planet and debris disc populations.

In both approaches, the solids in single-star class II discs are barely adequate to account for the solids contained in most of the known populations of planets (giant planets within 10 AU, super-Earths and Neptunes within 400 d) and debris discs. Moreover, the 5–30 M_{\oplus} population of planets at 0.5–10 AU discovered by microlensing is too numerous (at their reported incidence rate) to explain with the known reservoirs of T Tauri disc solids (§4). The discrepancy between the solid mass budgets of planets and class II discs implies that planet formation is already underway in the class II phase.

There are three main uncertainties in our analysis: (i) large errors in the incidence rates for 5–30 M_{\oplus} microlensing planets, (ii) uncertain solid core masses for Neptunes and

gas giants at 1–20 AU, and (iii) the reliability of disc masses from the simple optically thin estimate (eq. [4]). Lower incidence rates, smaller core masses, and larger disc masses would reduce the shortfall. While a clear preference for a significant microlensing rate is already apparent, the incidence rate would have to be reduced by a factor of 5–6 (from 52–62% to 10%) to eliminate the discrepancy. Further work to refine the incidence rate of the microlensing population would therefore be valuable to confirm the apparent shortfall.

The observed correlation between planet incidence rate and stellar metallicity appears to favor core accretion as the dominant pathway for the radial velocity planet population within a few AU (Fischer & Valenti 2005; Mayor et al. 2011; Miller & Fortney 2011). Thus, the large core masses we adopt seem reasonable. However, a similar analysis of the properties of the (5–30 M_{\oplus} , 1–10 AU) microlensing planet population would be valuable in determining whether the smaller solid core mass expected from the disc instability mechanism is preferred for planets at larger orbital radii.

Despite these uncertainties, our comparison of the solids in the known planets and single-star class II discs is fairly conservative. Other factors are likely to broaden the gap in the solid mass budget between discs and planets. Our comparison ignores the population of discless class III sources, the likely inefficiency of planet formation (factor > 2), and planet populations yet to be discovered (§5.2).

For these reasons, it seems difficult to escape the conclusion that planet formation is already underway in class II discs. This conclusion can be avoided only if the microlensing planets make a negligible contribution to the solid mass budget and none of the exacerbating factors (§5.2) play a significant role. If this extreme set of conditions is true, we would still conclude planet formation must be extremely frugal—all existing solids in class II discs will be turned into planets without loss. If this is the case, it is important to reconsider planet formation scenarios that are profligate in their use of disc material and rely on *only* the most massive class II discs to form known exoplanets. Because it does not require extreme assumptions, it seems more likely that the original interpretation is correct: planet formation begins early, and the comparison between the solids in class II discs and in known planetary systems provides a clear constraint on the epoch of planetesimal and planet formation.

ACKNOWLEDGMENTS

We thank Sean Andrews, Til Birnstiel, Ben Bromley, Margaret Geller, John Johnson, and Hubert Klahr for valuable discussions and comments on the manuscript. We also thank the referee for a helpful report that improved the clarity of the manuscript. Portions of this project were supported by the *NASA Astrophysics Theory and Origins of Solar Systems* programs through grant NNX10AF35G, the *NASA Outer Planets Program* through grant NNX11AM37G, and by the Institute for Theory and Computation at the Harvard-Smithsonian Center for Astrophysics.

REFERENCES

- Adachi, I., Hayashi, C., & Nakazawa, K. 1976, *Progress of Theoretical Physics*, 56, 1756
- Adams, F. C., Lada, C. J., & Shu, F. H. 1987, *ApJ*, 312, 788
- Agnor, C., & Asphaug, E. 2004, *ApJL*, 613, L157
- Andrews, S. M., Rosenfeld, K. A., Kraus, A. L., & Wilner, D. J. 2013, *ApJ*, 771, 129
- Andrews, S. M., & Williams, J. P. 2005, *ApJ*, 631, 1134
- . 2007, *ApJ*, 671, 1800
- Andrews, S. M., Wilner, D. J., Espaillat, C., Hughes, A. M., Dullemond, C. P., McClure, M. K., Qi, C., & Brown, J. M. 2011, *ApJ*, 732, 42
- Andrews, S. M., Wilner, D. J., Hughes, A. M., Qi, C., & Dullemond, C. P. 2009, *ApJ*, 700, 1502
- . 2010, *ApJ*, 723, 1241
- Armitage, P. J. 2003, *ApJL*, 582, L47
- Asphaug, E., Agnor, C. B., & Williams, Q. 2006, *Nature*, 439, 155
- Aumann, H. H., et al. 1984, *ApJL*, 278, L23
- Backman, D. E., & Paresce, F. 1993, in *Protostars and Planets III*, ed. E. H. Levy & J. I. Lunine, 1253–1304
- Batalha, N. M., et al. 2013, *ApJS*, 204, 24
- Beckwith, S. V. W., & Sargent, A. I. 1993, in *Protostars and Planets III*, ed. E. H. Levy & J. I. Lunine, 521–541
- Bertout, C., Siess, L., & Cabrit, S. 2007, *A&A*, 473, L21
- Biller, B. A., et al. 2013, *ApJ*, 777, 160
- Birnstiel, T., & Andrews, S. M. 2014, *ApJ*, 780, 153
- Birnstiel, T., Andrews, S. M., & Ercolano, B. 2012, *A&A*, 544, A79
- Birnstiel, T., Dullemond, C. P., & Brauer, F. 2010, *A&A*, 513, A79+
- Bizzarro, M., Baker, J. A., Haack, H., & Lundgaard, K. L. 2005, *ApJL*, 632, L41
- Bonsor, A., Kennedy, G. M., Wyatt, M. C., Johnson, J. A., & Sibthorpe, B. 2014, *MNRAS*, 437, 3288
- Boss, A. P. 2000, *ApJL*, 536, L101
- . 2005, *ApJ*, 629, 535
- Brauer, F., Dullemond, C. P., & Henning, T. 2008, *A&A*, 480, 859
- Bromley, B. C., & Kenyon, S. J. 2011, *ApJ*, 731, 101
- Bryden, G., et al. 2006, *ApJ*, 636, 1098
- Burke, C. J., et al. 2014, *ApJS*, 210, 19
- Carpenter, J. M., et al. 2009, *ApJS*, 181, 197
- Cassan, A., et al. 2012, *Nature*, 481, 167
- Chambers, J. 2008, *Icarus*, 198, 256
- Chambers, J. E. 2014, *Icarus*, 233, 83
- Chen, C. H., Mittal, T., Kuchner, M., Forrest, W. J., Lisse, C. M., Manoj, P., Sargent, B. A., & Watson, D. M. 2014, *ApJS*, 211, 25
- Chiang, E., & Laughlin, G. 2013, *MNRAS*, 431, 3444
- Chiang, E., & Youdin, A. N. 2010, *Annual Review of Earth and Planetary Sciences*, 38, 493
- Cieza, L. A., et al. 2013, *ApJ*, 762, 100
- Clanton, C., & Gaudi, S. 2014, *ArXiv e-prints*
- Clarke, C. J. 2009, *MNRAS*, 396, 1066
- Clarke, C. J., & Lodato, G. 2009, *MNRAS*, 398, L6
- Cohen, M., & Kuhl, L. V. 1979, *ApJS*, 41, 743
- Coleman, G. A. L., & Nelson, R. P. 2014, *ArXiv e-prints*
- Cumming, A., Butler, R. P., Marcy, G. W., Vogt, S. S., Wright, J. T., & Fischer, D. A. 2008, *PASP*, 120, 531
- Currie, T., Daemgen, S., Debes, J., Lafreniere, D., Itoh, Y., Jayawardhana, R., Ratzka, T., & Correia, S. 2014, *ApJL*, 780, L30
- Currie, T., Kenyon, S. J., Rieke, G., Balog, Z., & Bromley, B. C. 2007, *ApJL*, 663, L105
- Currie, T., Lada, C. J., Plavchan, P., Robitaille, T. P., Irwin, J., & Kenyon, S. J. 2009, *ApJ*, 698, 1
- Dauphas, N., & Chaussidon, M. 2011, *Annual Review of Earth and Planetary Sciences*, 39, 351
- Dauphas, N., & Pourmand, A. 2011, *Nature*, 473, 489
- Dawson, R. I., & Murray-Clay, R. 2012, *ApJ*, 750, 43
- Desch, S. J. 2007, *ApJ*, 671, 878
- Dittrich, K., Klahr, H., & Johansen, A. 2013, *ApJ*, 763, 117
- Dodson-Robinson, S. E., Bodenheimer, P., Laughlin, G., Willacy, K., Turner, N. J., & Beichman, C. A. 2008, *ApJL*, 688, L99
- Dodson-Robinson, S. E., Willacy, K., Bodenheimer, P., Turner, N. J., & Beichman, C. A. 2009, *Icarus*, 200, 672
- Dong, S., & Zhu, Z. 2013, *ApJ*, 778, 53
- Eiroa, C., et al. 2013, *A&A*, 555, A11
- Enoch, B., Collier Cameron, A., & Horne, K. 2012, *A&A*, 540, A99
- Espaillat, C., et al. 2014, *ArXiv e-prints*
- Fabrycky, D. C., et al. 2014, *ApJ*, 790, 146
- Fischer, D. A., & Valenti, J. 2005, *ApJ*, 622, 1102
- Fogg, M. J., & Nelson, R. P. 2009, *A&A*, 498, 575
- Foreman-Mackey, D., Hogg, D. W., & Morton, T. D. 2014, *ArXiv e-prints*
- Frank, A., et al. 2014, *ArXiv e-prints*
- Fressin, F., et al. 2013, *ApJ*, 766, 81
- Garaud, P., Meru, F., Galvagni, M., & Olczak, C. 2013, *ApJ*, 764, 146
- Gáspár, A., Rieke, G. H., & Balog, Z. 2013, *ApJ*, 768, 25
- Goldreich, P., & Ward, W. R. 1973, *ApJ*, 183, 1051
- Gould, A., et al. 2006, *ApJL*, 644, L37
- . 2010, *ApJ*, 720, 1073
- Greaves, J. S., & Rice, W. K. M. 2010, *MNRAS*, 407, 1981
- . 2011, *MNRAS*, 412, L88
- Greaves, J. S., & Wyatt, M. C. 2010, *MNRAS*, 404, 1944
- Güdel, M., Padgett, D. L., & Dougados, C. 2007, *Protostars and Planets V*, 329
- Habing, H. J., et al. 2001, *A&A*, 365, 545
- Haisch, Jr., K. E., Lada, E. A., & Lada, C. J. 2001, *ApJL*, 553, L153
- Hansen, B. M. S., & Murray, N. 2012, *ApJ*, 751, 158
- . 2013, *ApJ*, 775, 53
- Harris, R. J., Andrews, S. M., Wilner, D. J., & Kraus, A. L. 2012, *ApJ*, 751, 115
- Hartmann, L., Calvet, N., Gullbring, E., & D’Alessio, P. 1998, *ApJ*, 495, 385
- Hartmann, L., & Kenyon, S. J. 1996, *ARA&A*, 34, 207
- Hayashi, C. 1981, *Progress of Theoretical Physics Supplement*, 70, 35
- Helled, R., et al. 2013, *ArXiv e-prints*
- Herbst, W. 2008, *Star Formation in IC 348*, ed. B. Reipurth (San Francisco: Astronomical Society of the Pacific), 372
- Hernández, J., et al. 2007, *ApJ*, 662, 1067
- Howard, A. W. 2013, *Science*, 340, 572
- Howard, A. W., et al. 2010, *Science*, 330, 653
- . 2012, *ApJS*, 201, 15
- Hueso, R., & Guillot, T. 2005, *A&A*, 442, 703

- Hugot, E., Ferrari, M., El Hadi, K., Costille, A., Dohlen, K., Rabou, P., Puget, P., & Beuzit, J. L. 2012, *A&A*, 538, A139
- Ida, S., & Lin, D. N. C. 2005, *ApJ*, 626, 1045
- . 2008a, *ApJ*, 673, 487
- . 2008b, *ApJ*, 685, 584
- Janson, M., Bonavita, M., Klahr, H., & Lafrenière, D. 2012, *ApJ*, 745, 4
- Jensen, E. L. N., & Akeson, R. L. 2003, *ApJ*, 584, 875
- Johansen, A., Oishi, J. S., Mac Low, M.-M., Klahr, H., Henning, T., & Youdin, A. 2007, *Nature*, 448, 1022
- Johansen, A., Youdin, A., & Mac Low, M.-M. 2009, *ApJL*, 704, L75
- Johnson, J. A., Aller, K. M., Howard, A. W., & Crepp, J. R. 2010, *PASP*, 122, 905
- Jovanovic, N., et al. 2013, in *Proceedings of the Third AO4ELT Conference*, ed. S. Esposito & L. Fini
- Jurić, M., & Tremaine, S. 2008, *ApJ*, 686, 603
- Kennedy, G. M., & Kenyon, S. J. 2008, *ApJ*, 682, 1264
- . 2009, *ApJ*, 695, 1210
- Kennedy, G. M., & Wyatt, M. C. 2010, *MNRAS*, 405, 1253
- Kenyon, S. J., & Bromley, B. C. 2004, *ApJL*, 602, L133
- . 2008, *ApJS*, 179, 451
- . 2010, *ApJS*, 188, 242
- Kenyon, S. J., Gómez, M., & Whitney, B. A. 2008, in *Handbook of Star Forming Regions, Volume I*, ed. Reipurth, B. (San Francisco: Astronomical Society of the Pacific), 405–+
- Kenyon, S. J., & Hartmann, L. 1995, *ApJS*, 101, 117
- Kleine, T., et al. 2009, *Geo. Cosm. Acta*, 73, 5150
- Kratter, K. M., Murray-Clay, R. A., & Youdin, A. N. 2010, *ApJ*, 710, 1375
- Kraus, A. L., & Ireland, M. J. 2012, *ApJ*, 745, 5
- Kraus, A. L., Ireland, M. J., Martinache, F., & Hillenbrand, L. A. 2011, *ApJ*, 731, 8
- Krivov, A. V., Müller, S., Löhne, T., & Mutschke, H. 2008, *ApJ*, 687, 608
- Lagrange, A.-M., et al. 2010, *Science*, 329, 57
- Laibe, G. 2014, *MNRAS*, 437, 3037
- Laibe, G., Gonzalez, J.-F., & Maddison, S. T. 2012, *A&A*, 537, A61
- Lambrechts, M., & Johansen, A. 2012, *A&A*, 544, A32
- Lissauer, J. J., et al. 2011, *ApJS*, 197, 8
- Lopez, E. D., & Fortney, J. J. 2013, *ArXiv e-prints*
- Luhman, K. L., Allen, P. R., Espaillat, C., Hartmann, L., & Calvet, N. 2010, *ApJS*, 186, 111
- Macintosh, B., et al. 2014, *ArXiv e-prints*
- Malhotra, R. 1995, *AJ*, 110, 420
- Mamajek, E. E. 2009, in *American Institute of Physics Conference Series*, Vol. 1158, American Institute of Physics Conference Series, ed. T. Usuda, M. Tamura, & M. Ishii, 3–10
- Mann, A. W., Gaidos, E., & Gaudi, B. S. 2010, *ApJ*, 719, 1454
- Marois, C., Macintosh, B., Barman, T., Zuckerman, B., Song, I., Patience, J., Lafrenière, D., & Doyon, R. 2008, *Science*, 322, 1348
- Marshall, J. P., et al. 2014, *A&A*, 565, A15
- Matthews, B. C., Krivov, A. V., Wyatt, M. C., Bryden, G., & Eiroa, C. 2014, *ArXiv e-prints*
- Mayor, M., et al. 2011, *ArXiv e-prints*
- Melis, C., Zuckerman, B., Rhee, J. H., & Song, I. 2010, *ApJL*, 717, L57
- Miller, N., & Fortney, J. J. 2011, *ApJL*, 736, L29
- Morbidelli, A. 2013, *Dynamical Evolution of Planetary Systems*, ed. T. D. Oswalt, L. M. French, & P. Kalas (Dordrecht: Springer Science & Business Media), 63
- Morton, T. D., & Swift, J. J. 2013, *ArXiv e-prints*
- Najita, J. R., & Shu, F. H. 1994, *ApJ*, 429, 808
- Nakagawa, Y., Sekiya, M., & Hayashi, C. 1986, *Icarus*, 67, 375
- Nielsen, E. L., & Close, L. M. 2010, *ApJ*, 717, 878
- Offner, S. S. R., & McKee, C. F. 2011, *ApJ*, 736, 53
- Ormel, C. W., & Klahr, H. H. 2010, *A&A*, 520, A43
- Osterloh, M., & Beckwith, S. V. W. 1995, *ApJ*, 439, 288
- Pérez, L. M., et al. 2012, *ApJL*, 760, L17
- Petigura, E. A., Marcy, G. W., & Howard, A. W. 2013, *ArXiv e-prints*
- Pinte, C., & Laibe, G. 2014, *A&A*, 565, A129
- Piso, A.-M. A., & Youdin, A. N. 2014, *ApJ*, 786, 21
- Pollack, J. B., Hubickyj, O., Bodenheimer, P., Lissauer, J. J., Podolak, M., & Greenzweig, Y. 1996, *Icarus*, 124, 62
- Preibisch, T., & Mamajek, E. 2008, *The Nearest OB Association: Scorpius-Centaurus (Sco OB2)*, ed. B. Reipurth (San Francisco: Astronomical Society of the Pacific), 235
- Rafikov, R. R. 2003, *AJ*, 126, 2529
- . 2005, *ApJL*, 621, L69
- . 2006, *ApJ*, 648, 666
- . 2011, *ApJ*, 727, 86
- Rasio, F. A., & Ford, E. B. 1996, *Science*, 274, 954
- Raymond, S. N., Armitage, P. J., & Gorelick, N. 2010, *ApJ*, 711, 772
- Raymond, S. N., & Cossou, C. 2014, *MNRAS*, 440, L11
- Raymond, S. N., et al. 2011, *ArXiv e-prints*
- Rhee, J. H., Song, I., & Zuckerman, B. 2008, *ApJ*, 675, 777
- Rhee, J. H., Song, I., Zuckerman, B., & McElwain, M. 2007, *ApJ*, 660, 1556
- Rice, W. K. M., & Armitage, P. J. 2009, *MNRAS*, 396, 2228
- Rice, W. K. M., Lodato, G., Pringle, J. E., Armitage, P. J., & Bonnell, I. A. 2004, *MNRAS*, 355, 543
- . 2006, *MNRAS*, 372, L9
- Rieke, G. H., et al. 2005, *ApJ*, 620, 1010
- Rogers, L. A., Bodenheimer, P., Lissauer, J. J., & Seager, S. 2011, *ApJ*, 738, 59
- Rowe, J. F., et al. 2014, *ApJ*, 784, 45
- Schulz, T., Münker, C., Palme, H., & Mezger, K. 2009, *Earth and Planetary Science Letters*, 280, 185
- Seager, S., Kuchner, M., Hier-Majumder, C. A., & Militzer, B. 2007, *ApJ*, 669, 1279
- Sierchio, J. M., Rieke, G. H., Su, K. Y. L., & Gáspár, A. 2014, *ApJ*, 785, 33
- Siess, L., Dufour, E., & Forestini, M. 2000, *A&A*, 358, 593
- Smith, B. A., & Terrile, R. J. 1984, *Science*, 226, 1421
- Stark, C. C., & Kuchner, M. J. 2009, *ApJ*, 707, 543
- Sugiura, N., & Fujiya, W. 2014, *Meteoritics and Planetary Science*, 49, 772
- Sumi, T., et al. 2011, *Nature*, 473, 349
- Thebault, P., Kral, Q., & Ertel, S. 2012, *A&A*, 547, A92
- Torres, G., Winn, J. N., & Holman, M. J. 2008, *ApJ*, 677, 1324

- Trilling, D. E., Benz, W., Guillot, T., Lunine, J. I., Hubbard, W. B., & Burrows, A. 1998, *ApJ*, 500, 428
- Trilling, D. E., et al. 2007, *ApJ*, 658, 1289
- . 2008, *ApJ*, 674, 1086
- Turner, N. J., Fromang, S., Gammie, C., Klahr, H., Lesur, G., Wardle, M., & Bai, X.-N. 2014, *ArXiv e-prints*
- Vorobyov, E. I. 2011, *ApJ*, 729, 146
- Ward, W. R. 1997, *Icarus*, 126, 261
- Weidenschilling, S. J. 1977a, *MNRAS*, 180, 57
- . 1977b, *ApSS*, 51, 153
- . 1980, *Icarus*, 44, 172
- Weiss, L. M., & Marcy, G. W. 2014, *ApJL*, 783, L6
- Weiss, L. M., et al. 2013, *ApJ*, 768, 14
- Wetherill, G. W., & Stewart, G. R. 1993, *Icarus*, 106, 190
- Wilking, B. A., Gagné, M., & Allen, L. E. 2008, *Star Formation in the ρ Ophiuchi Molecular Cloud*, ed. B. Reipurth (San Francisco: Astronomical Society of the Pacific), 351
- Williams, J. P. 2012, *Meteoritics and Planetary Science*, 47, 1915
- Williams, J. P., & Cieza, L. A. 2011, *ARA&A*, 49, 67
- Wilner, D. J., Holman, M. J., Kuchner, M. J., & Ho, P. T. P. 2002, *ApJL*, 569, L115
- Windmark, F., Birnstiel, T., Ormel, C. W., & Dullemond, C. P. 2012, *A&A*, 544, L16
- Wyatt, M. C. 2008, *ARA&A*, 46, 339
- Wyatt, M. C., Dermott, S. F., Telesco, C. M., Fisher, R. S., Grogan, K., Holmes, E. K., & Piña, R. K. 1999, *ApJ*, 527, 918
- Yamamoto, K., et al. 2013, *PASJ*, 65, 90
- Youdin, A. N. 2011a, *ApJ*, 731, 99
- . 2011b, *ApJ*, 742, 38
- Youdin, A. N., & Chiang, E. I. 2004, *ApJ*, 601, 1109
- Youdin, A. N., & Goodman, J. 2005, *ApJ*, 620, 459
- Youdin, A. N., & Kenyon, S. J. 2013, *From Disks to Planets*, ed. T. D. Oswalt, L. M. French, & P. Kalas (Dordrecht: Springer Science & Business Media), 1

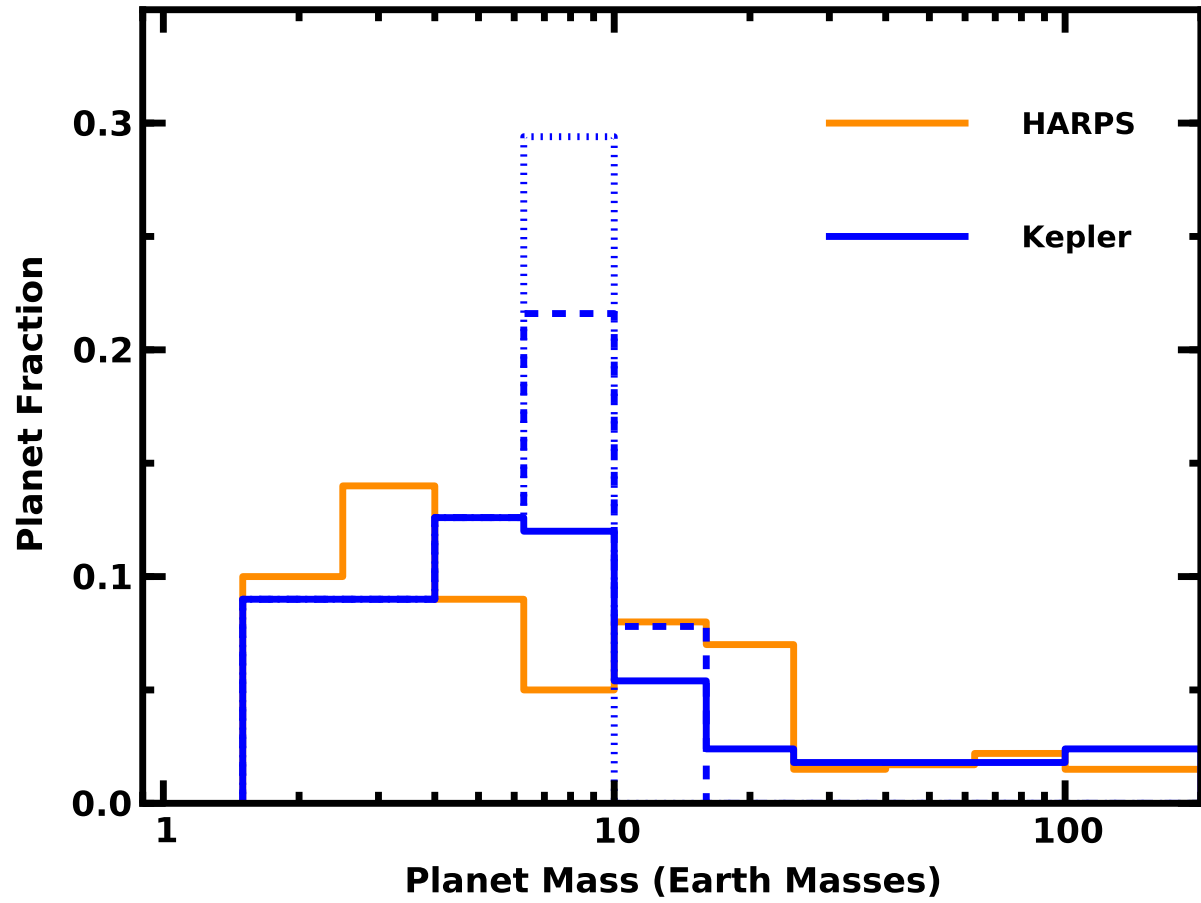


Figure 1. Differential incidence rates for exoplanets close to their host stars. As summarized in the legend, solid lines show rates for (i) *Kepler* planets with $P \leq 125$ d from this paper (blue line; see also Dong & Zhu 2013); and (ii) HARPS planets with $P \leq 100$ d (orange line; Mayor et al. 2011). Dotted (dashed) lines plot incidence rates for the solid mass in *Kepler* planets assuming core masses of $10 M_{\oplus}$ ($7.5\text{--}12.5 M_{\oplus}$).

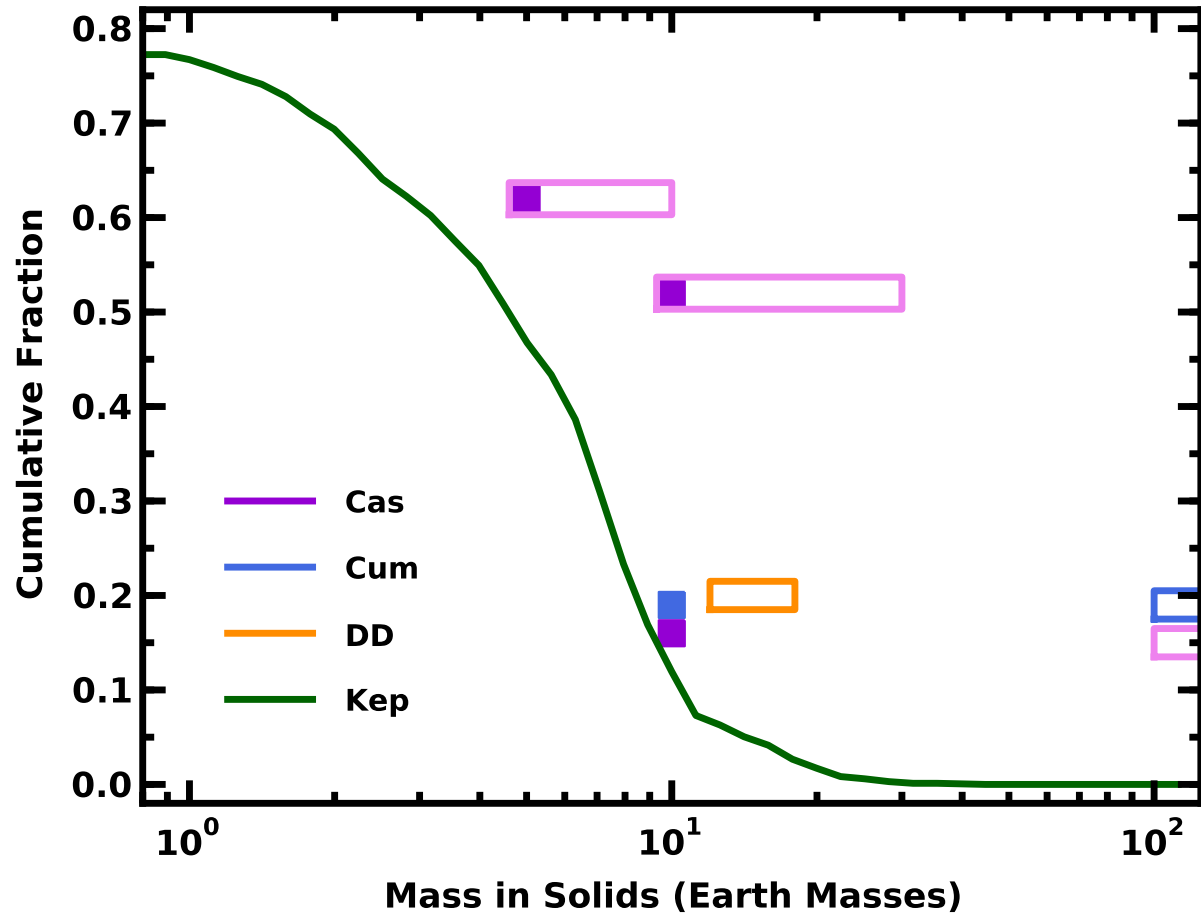


Figure 2. Differential incidence rates for debris discs (‘DD’; e.g., Eiroa et al. 2013) and exoplanets from *Kepler* (‘Kep’, this paper), microlensing (‘Cas’; Cassan et al. 2012), and radial velocities (‘Cum’; Cumming et al. 2008). Solid green curve: cumulative incidence rate for *Kepler* planets with $P \leq 400$ d. Violet boxes: differential rates for microlensing planets with $a = 0.5$ –10 AU. Open, light rectangles indicate the nominal mass range; dark, filled squares show the adopted mass in solids. Blue boxes: nominal mass range (open symbol) and adopted mass in solids (filled symbol) for gas giant planets with $a \leq 20$ AU inferred from radial velocity surveys. Orange rectangle: adopted range in solid mass at $a \geq 20$ AU for debris discs.

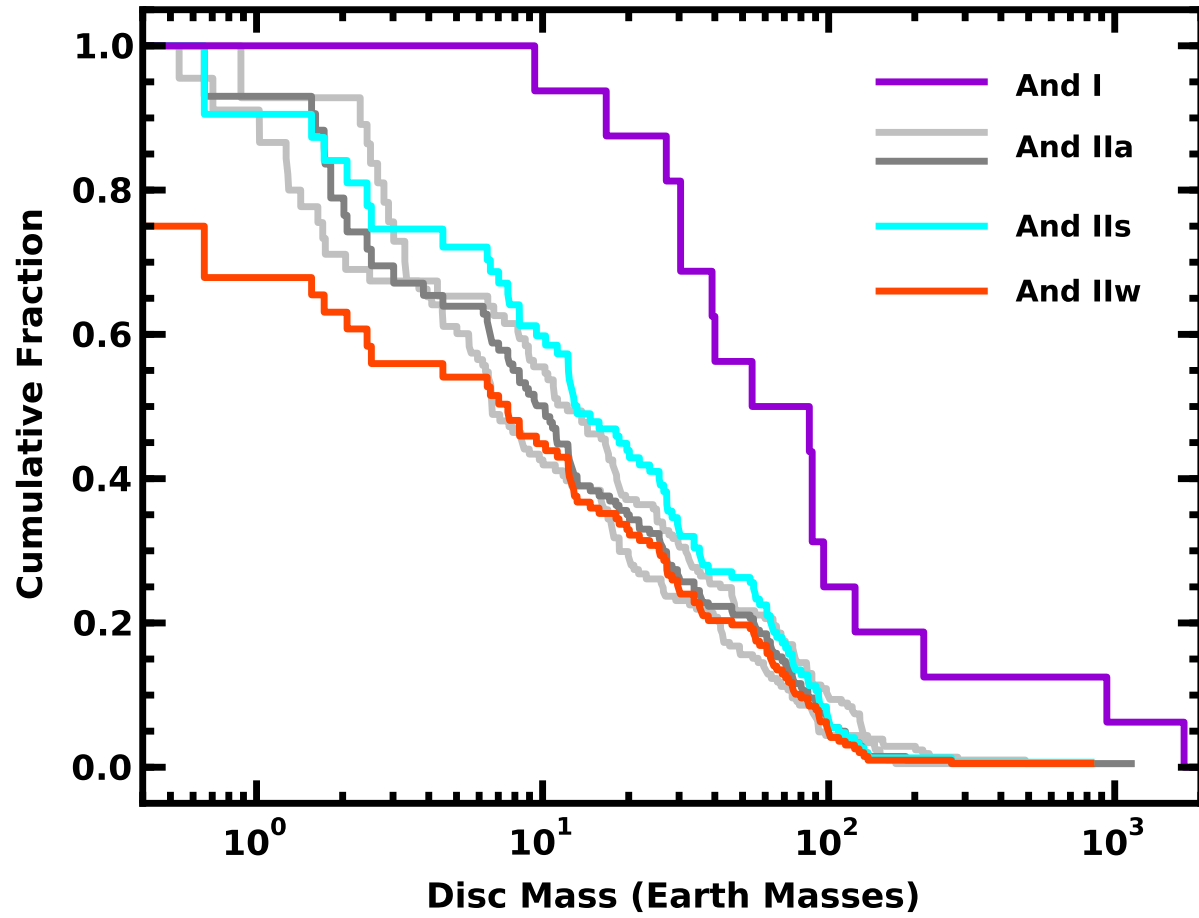


Figure 3. Cumulative mass distributions ($f(> M_d/M_*)$) for protoplanetary discs. Violet curve (‘And I’): class I sources from Andrews & Williams (2005). Grey curves (‘And IIa’): complete set of class II sources from Andrews et al. (2013) using three different calculations of the mass-luminosity-temperature relation for pre-main sequence stars (for details, see Andrews et al. 2013). Cyan curve (‘And IIs’): set of ‘single’ class II sources with the mass-luminosity-temperature relations from Andrews et al. (2013) and the Siess et al. (2000) evolutionary tracks. Red curve (‘And IIw’): class II + III sources assuming a 25% fraction of discless stars.

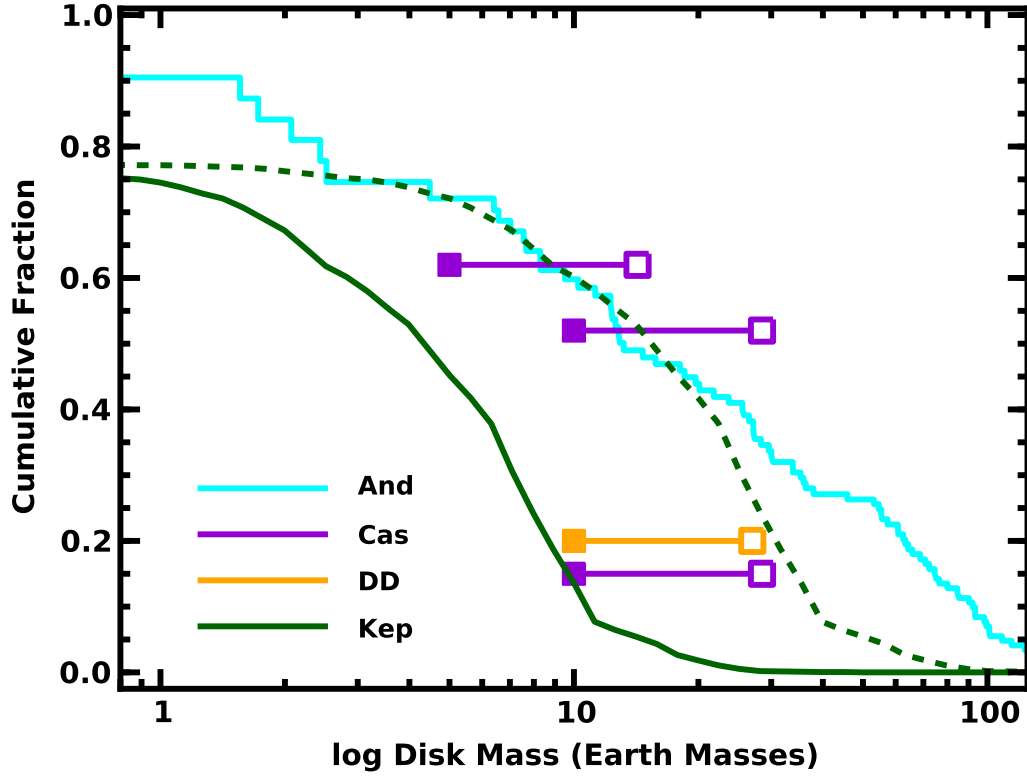


Figure 4. Mass distributions for protoplanetary discs. Cyan curve ('And'): observed mass distribution for single class II sources from Figure 3 (Andrews et al. 2013). Solid curve and filled symbols: observed mass distribution for *Kepler* planets with $P \leq 400$ d ('Kep'; green curve), debris discs ('DD'; orange box), and microlensing planets ('Cas'; violet boxes). Dashed curve and open symbols: required total disc masses $M_{tot,s}$ if $\Sigma \propto a^{-3/2}$ and if the above planets and debris discs arise from (i) $a \leq 4$ AU (dashed green curve, *Kepler* planets with $a \leq 1$ AU), (ii) $4 \text{ AU} \leq a \leq 20$ AU (open violet boxes, microlensing planets), and (iii) $a \geq 20$ AU (open orange box, debris discs).

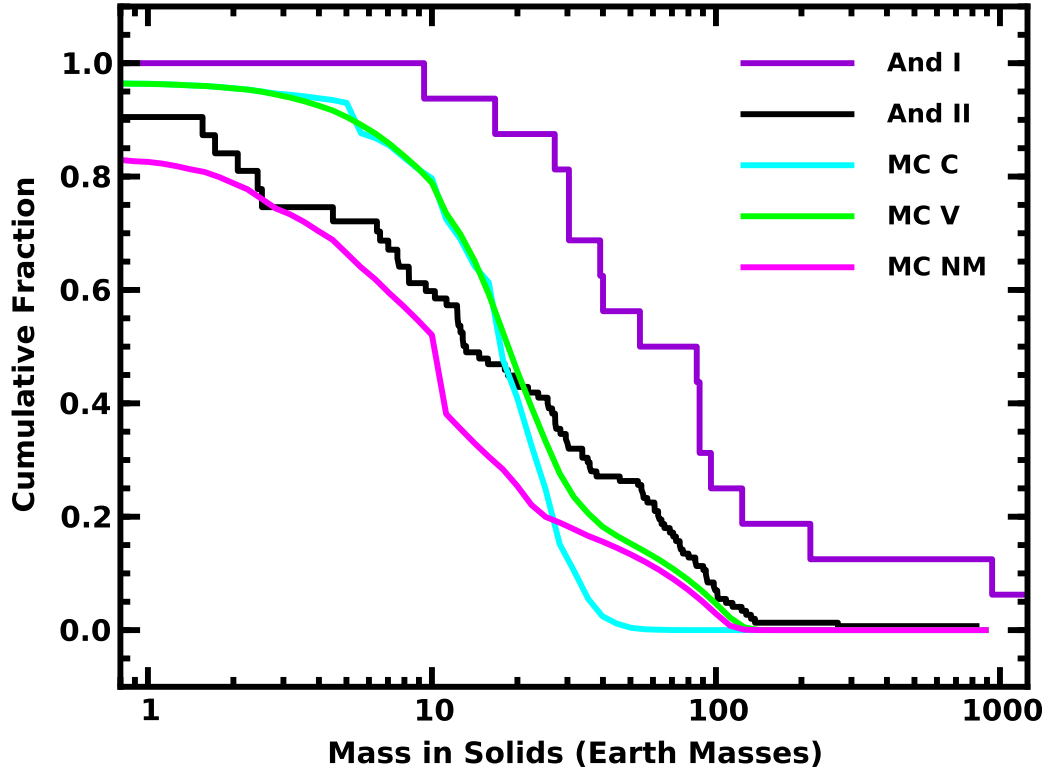


Figure 5. Comparison of incidence rates for exoplanets and protoplanetary discs. Violet (‘And I’; class I sources) and black (‘And II’; single class II sources) jagged curves: observed mass distributions for protoplanetary discs (Andrews et al. 2013). Cyan (‘MC C’; constant core mass model) and green (‘MC V’; variable core mass model) smooth curves: mass distributions calculated from the Monte Carlo model described in the text. Smooth magenta curve (‘MC NM’): mass distribution from the Monte Carlo model with a variable core mass but no 5–10 M_{\oplus} planets at 1–10 AU from microlensing. Although discs around T Tauri stars have enough mass to explain the frequency of debris discs beyond 20 AU, gas giants inside 20 AU, and *Kepler* planets inside 1 AU, they do not contain enough mass to explain the observed frequency of super-Earths detected in microlensing surveys. Disks around protostars have large enough reservoirs to explain the incidence rates for all known exoplanets.

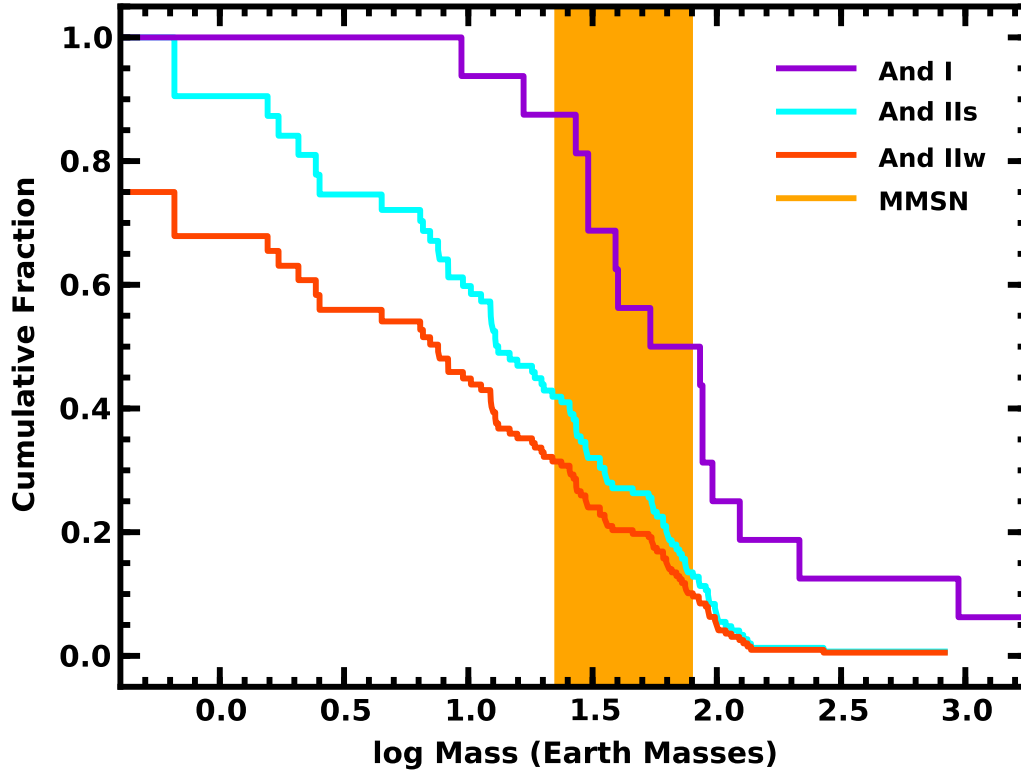


Figure 6. Comparison of the minimum mass solar nebula (MMSN) and ‘minimum mass exoplanet nebulae’ (MMEN) with the mass distributions of protoplanetary discs. The orange bar indicates the mass range for the MMSN and MMEN. Solid lines plot the mass distributions of the discs in class I protostars (‘And I’, upper violet curve), class II sources (‘And IIs’, middle cyan curve), and class II+III sources (‘And IIw’, lower red curve). The MMSN and MMEN lie well above the median disc mass of the class II and class II+III distributions.

This paper has been typeset from a \TeX / \LaTeX file prepared
by the author.